Nuclear and electron dynamics in the photodissociation of water

Peter Andresen, G. S. Ondrey, B. Titze, and Erhard W. Rothe

Citation: The Journal of Chemical Physics **80**, 2548 (1984); doi: 10.1063/1.447049
View online: http://dx.doi.org/10.1063/1.447049
View Table of Contents: http://scitation.aip.org/content/aip/journal/jcp/80/6?ver=pdfcov
Published by the AIP Publishing

Nuclear and electron dynamics in the photodissociation of water

Peter Andresen, G. S. Ondrey,[a),b)] and B. Titze
Max-Planck-Institut für Strömungsforschung, Böttingerstrasse 4-8, D 3400 Göttingen, Federal Republic of Germany

Erhard W. Rothe[a)]
Research Institute for Engineering Sciences and Department of Chemical Engineering, Wayne State University, Detroit, Michigan 48202

(Received 16 September 1983; accepted 17 November 1983)

The photodissociation of water in its first absorption band is studied by photolyzing H_2O at 157 nm with an excimer laser. This dissociation proceeds directly to produce the electronic ground states of H and OH. Both nascent internal state distributions and alignment of the product OH ($^2\Pi$) are probed by laser induced fluorescence. This is done with both warm (300 K) and cold (~ 10 K) water. About 88% of the excess energy is translation, 10% vibration, about 2% rotation. The first three vibrational levels 0, 1, 2 have population ratios 1:1:0.15, respectively. The rotational distributions depend strongly upon the H_2O temperature and are very different for the upper and lower energy components of the Λ doublets, which are measured via Q and P,R lines, respectively. For Q lines, the distributions can be described by rotational temperatures which are 930 K for warm and 475 K for cold water, a surprising difference. For P,R lines strong deviations from Boltzmann behavior are found for cold H_2O. The spin distribution is almost statistical. A strong J dependent Λ-doublet population inversion is found from cold H_2O, but there is no inversion from warm H_2O. The inversion provides a possible pump mechanism for the astronomical OH maser and is simply explained by approximate symmetry conservation. The orientation of the unpaired $p\pi$ lobe in OH in the upper Λ-doublet state is measured to be perpendicular to the OH rotation plane. The J dependence of the inversion is explained by Λ-doublet mixing in OH and quantitatively described in terms of the singly occupied $p\pi$-lobe in the excited water and the orientation of the corresponding singly occupied $p\pi$-lobe in OH. The alignment of OH is measured by polarizing both lasers. The large polarization effects are strongly dependent upon J and also upon the temperature of H_2O. It is shown that the dependence is related both to Λ-doublet mixing and hyperfine structure of OH. For the cold H_2O the data indicate, despite the strong J dependence of both polarization and Λ-doublet inversion, a completely planar dissociation process. It is shown that due to Λ-doublet mixing the transition moment of Π molecules has a J dependent angle relative to the OH rotation plane which approaches the high J limit at the same rate that the molecule shifts from Hund's case (a) to case (b). The model for the J dependence of the Λ-doublet population and the polarization is important for chemical reactions, surface scattering and other processes where Π molecules are analyzed with LIF.

I. INTRODUCTION

In the last few years it has been demonstrated that the use of lasers in photodissociation studies yields detailed information about the dynamics of such processes. Together with recent progress in the theoretical treatment of photodissociation it may be possible to extract detailed data about the potential energy surfaces involved. In this paper we will demonstrate how sensitive the experimental information can be to the parent temperatures and the electron and nuclear configurations.

Photodissociation can be considered as the second half of a collision, i.e., a scattering process on the final electronic surface.[1,2] Here an activated complex is prepared by the absorption of a photon by a ground state molecule rather than by the first half of a bimolecular collision. The photoabsorption results in a much narrower and well defined distribution of internuclear distances and energies in the complex than would be true for collision complexes where a large range of impact parameters contribute.

This complex can be even better defined by cooling the parent rotation in a nozzle beam, so as to excite molecules to a narrow range of initial quantum states, and/or preparing aligned complexes using polarized light. The products can be analyzed for distributions among quantum states, substates and kinetic energy and for alignment, with the use of laser-induced fluorescence.

In this paper we investigate in detail the photodissociation of H_2O at 157 nm:

$$H_2O(^1A_1) + h\nu(157\,\text{nm}) \rightarrow H_2O(^1B_1) \rightarrow OH(^2\Pi) + H(^2S),$$
$$\Delta E_0^0 = 2.89\ \text{eV},$$

which gives OH in the electronic ground state exclusively.[3,4] This is a very simple and elementary process, because it is one of the very few cases where a dissociation is direct and occurs on a single well-defined potential energy surface. The number of electrons involved is so small that *ab initio* quan-

[a)] Guests at MPI, where experiments were conducted.
[b)] Present address, Department of Chemistry, Gannon University, Erie, PA 16502.

 0021-9606/84/062548-22$02.10

tum calculations can be done even for excited states of H_2O. The fragmentation can be treated as a scattering process and full quantum calculations can yield product energy distribution and fragment alignment. This is a fortunate case where a comparison of experiment and theory is possible, and therefore we believe that the photodissociation of H_2O at 157 nm may serve as a model system for the dynamics of such simple fragmentation processes.

Although there have been many studies of the photodissociation of water, only one previous work[5] was done in the first absorption band. Most of the dissociation studies were done at wavelengths in the second absorption band where electronically excited OH[6,7] is formed.

In this paper we present the measured nascent internal state distributions of $OH(^2\Pi)$ for rotational and vibrational levels for both spin states and the Λ-doublet sublevels. In addition both lasers could be linearly polarized and the alignment of OH angular momenta relative to the initially photoselected H_2O plane was determined. The influence of the internal rotational temperature of the parent on both the state distribution and alignment of the product was studied by cooling the H_2O in a nozzle expansion.

Even for this elementary process, surprising results were found which will demonstrate the high selectivity of photodissociation events. Both rotational and vibrational distributions are sensitive to details of the potential energy surface and should enable us to determine the topology of a repulsive surface by a comparison of experiment and theory.

The most important aspect of this experiment, however, is related to the Λ-doublet population and the polarization. First, we find a strong population inversion in the Λ doublets of OH, suggesting an appealing explanation of the pump mechanism of the astronomical OH maser: photodissociation of H_2O in the VUV.[8] It is the first experimental observation of a population *inversion* in OH resulting from either collisions or photodissociation. The large inversion is caused by symmetry conservation during the dissociation. If the H_2O is rotating prior to dissociation the Λ-doublet population becomes statistical, indicating that the Born–Oppenheimer coupling is important in the experiment.

The dissociation of cold H_2O is completely planar (i.e., OH rotates in the original H_2O plane after dissociation), giving maximum possible alignment of OH and maximum possible Λ-doublet-population inversion. Nevertheless both polarization and Λ-doublet inversion show a strong dependence upon the final OH-angular momenta J_{OH}.

The J_{OH} dependence of the Λ-doublet population is explained by *Λ-doublet mixing* in the free OH. The simple model applied here should also be applicable to chemical reactions and explain the J dependence of the Λ-doublet population found there. An analysis of the Λ-doublet population yields information about the planarity of such processes.

The polarization experiments yield complementary information about the dissociation. Whereas the Λ-doublet population depends only upon electron anisotropies in the molecular frame, the polarization experiment measures nuclear anisotropies in the laboratory frame. Although the raw data have a strong J_{OH} dependence in the polarization experiment, this is compatible with complete alignment of OH. The strong J_{OH} dependence is due to (a) the hyperfine structure of OH and (b) the Λ-doublet mixing in the free OH.

The analysis of both Λ-doublet population and polarization presented here should become a useful tool for the interpretation of chemical reactions, surface scattering and photodissociation in which Π molecules are involved.

II. OVERVIEW OF THE DISSOCIATION PROCESS

In this section we will discuss the implications of a completely planar dissociation process—which is only found for the dissociation of internally cold H_2O—upon the Λ-doublet population and the OH-product alignment. This is done in order to provide a foundation for the remaining part of this paper. First we will briefly and pictorially describe the electronic orbitals involved in the fragmentation from H_2O. Then we will explain the basic idea of the polarization experiment.

The electronic ground state of the water molecule, which has only ten electrons, is a textbook[9,10] example for the use of delocalized orbitals. Its electronic configuration in the ground state $^1A_1$ is described in terms of molecular orbitals by $(1a_1)^2(2a_1)^2(1b_2)^2(3a_1)^2(1b_1)^2$. These orbitals[11] are shown in Fig. 1, and are described there.

In the first absorption band[3,12] of $H_2O(^1B_1 \rightarrow {}^1A_1)$ the most loosely bound electron $1b_1$ is raised to the lowest antibonding orbital $4a_1^*$. This process is shown schematically in Fig. 2. To the left of the ground state ($^1A_1$) potential well is a structure which displays the doubly occupied $1b_1$ orbital

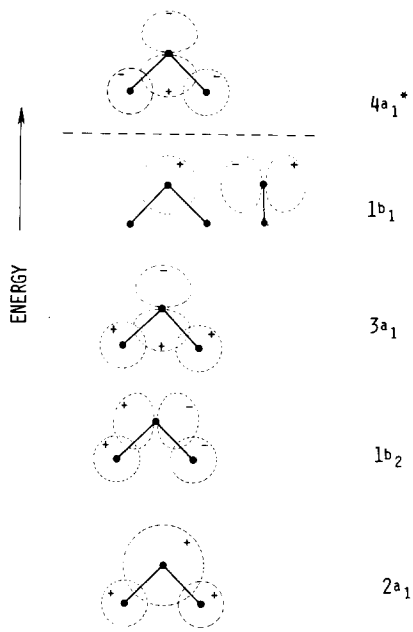

FIG. 1. H_2O molecular orbitals (after Herzberg, Ref. 11). The $1a_1$ orbital (not shown) is, in essence, the 1*s* orbital of O. The $2a_1$ is mainly O (2*s*) with small mixtures of O($2p_y$) and the symmetric combination H (1*s*) + H′(1*s*). The $3a_1$ is strongly bonding and is mainly O($2p_y$) with a mixture of O(2*s*) and H(1*s*) + H′(1*s*). The $1b_2$ orbital also bonds strongly and is a mixture of O($2p_z$) and the antisymmetric combination H (1*s*)-H′(1*s*). The $1b_1$ orbital is entirely described by the nonbonding O($2p_x$). In addition to these ground state orbitals of H_2O, the antibonding $4a_1^*$ is also shown. This orbital is a mixture of O(2*s*), O($2p_y$), and the symmetric combination H(1*s*) + H′(1*s*).

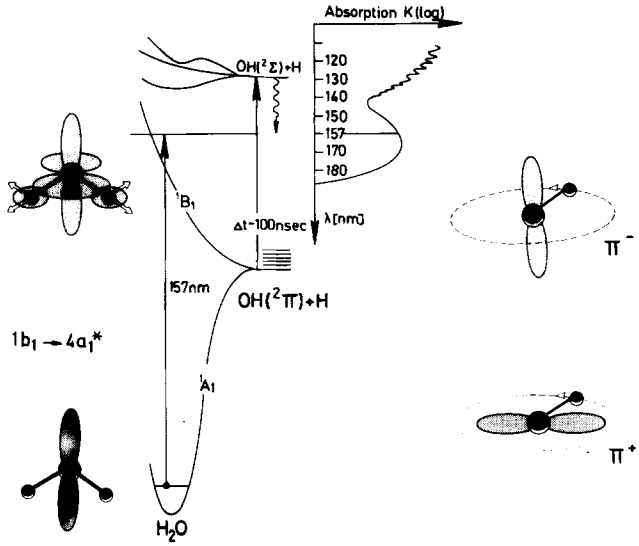

FIG. 2. Schematics of OH excitation and subsequent dissociation. In the transition $H_2O(^1B_1 \rightarrow {}^1A_1)$ at 157 nm one electron is moved from the filled nonbonding $1b_1$ orbital (lower left) to the $4a_1^*$ antibonding orbital (upper left) and leaves one free unpaired electron in the $1b_1$ orbital. The corresponding first (and also second) absorption band of water are shown at the right side. The nascent $OH(^2\Pi)$ is state selectively probed by LIF via the $OH(^2\Sigma)$ state. The two idealized orientations of the unpaired electron (previously designated $1b_1$ in H_2O) relative to OH angular momentum give the two different Π^- and Π^+-Λ-doublet states of OH (shown right).

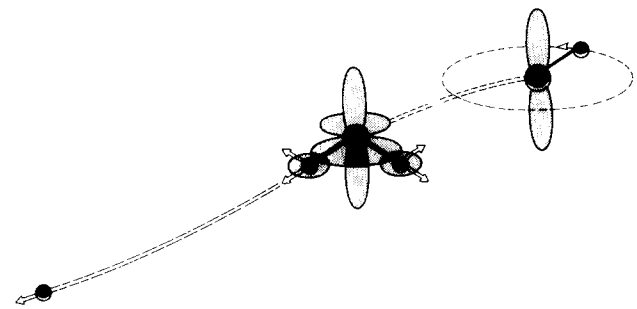

FIG. 3. Pictorial view of the dissociation process. In the middle is the electronic configuration of water in the excited $^1B_1$ state after photon absorption. At the left and right side are the H and OH that are leaving the complex. Note the direction of the $1b_1$ orbital in the H_2O is parallel to the $p\pi$ lobe in the OH. The arrows indicate forces relevant to rotational and vibrational excitation.

perpendicular to the H_2O plane. The 157 nm photon causes a transition to the repulsive upper state ($^1B_1$) which is represented by the singly occupied (less-shaded) $1b_1$ orbital which remains perpendicular to the H_2O plane, and the $4a_1^*$ orbital which lies in the plane and which has nodes between the O and H atoms.

Quantum calculations[13] show that there are no crossings with nearby singlet states, and that the formation of $O(^1D) + H_2$, although exoergic, is forbidden by a potential barrier. Thus the H_2O dissociates along the well defined $^1B_1$ potential surface to the products $OH(^2\Pi) + H$.[4] The nascent OH is detected by LIF via the $OH(^2\Sigma$–$^2\Pi)$ absorption band. These features are indicated in Fig. 2, where the absorption spectrum of H_2O is displayed at the right. At 157 nm, we are close to the maximum of the featureless first absorption band, which is typical for a repulsive electronic state. The formation of electronically excited $OH(^2\Sigma)$ becomes possible only at shorter wavelengths and belongs to the second absorption band. As a Π molecule, OH has a half filled $p\pi$ lobe perpendicular to its internuclear axis. Two possible orientations of this $p\pi$ lobe relative to the OH rotation plane are shown at the right of Fig. 2. These two orientations can be identified (in the high J limit) by the two Λ-doublet states Π^- and Π^+.

Figure 3 shows the decay of the excited $^1B_1$ complex in a pictorial view. The strong forces, indicated by the arrows, are due to the $4a_1^*$ orbital and act in the H_2O plane. As a consequence the OH will rotate in the original H_2O plane. The $1b_1$ orbital of H_2O (i.e., the atomic $2p$ orbital) resembles closely the $p\pi$ orbital of OH, and a casual look at the figure suggests that, in the absence of other interactions the orbital will remain where it was in the H_2O, namely perpendicular to the H_2O plane. Another explanation for forming only the Π^- configuration that is displayed in Fig. 3 is based on the symmetry of these orbitals relative to the rotation plane: Whereas both $1b_1$ and the Π^- configuration are antisymmetric, the Π^+ configuration is symmetric.

The basic concept of the polarization experiment, although simplified, will be discussed here with the use of Fig. 4. The upper part shows the experimental geometry with both laser beams along X, the H_2O nozzle beam along Z, and the fluorescence detection along Y.

Also shown is an arbitrary orientation of an H_2O plane together with the transition moment vector μ. At 157 nm, in the first absorption band, μ is perpendicular to the plane because charge is transferred from an orbital perpendicular to the plane ($1b_1$) to an in-plane orbital ($4a_1^*$).[11] For simplicity we assume the electric vector ϵ_D of the linearly polarized excimer laser to be along Z. For the absorption only the component of ϵ_D along μ is important, so that the excitation probability is given by

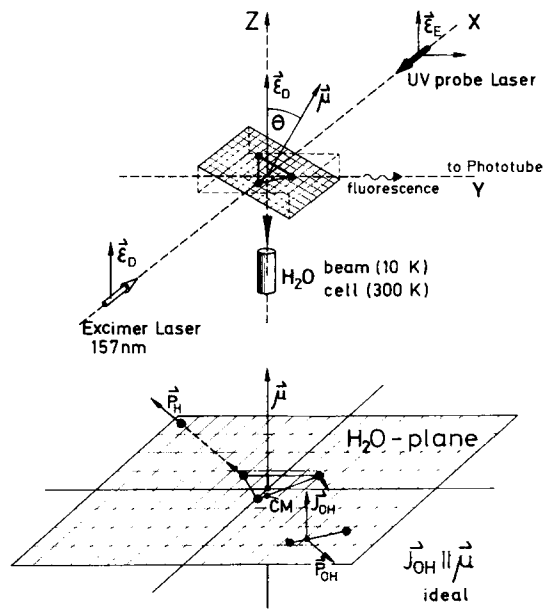

FIG. 4. Principle of the idealized polarization experiment, showing relationships of laser electric vectors to a molecular plane of arbitrary orientation (see the text).

$$|\epsilon_D \cdot \mu|^2 \propto \cos^2 \theta,$$

where θ is the angle between μ and ϵ_D. This implies that we select molecules for dissociation whose μ are preferentially aligned—with a $\cos^2 \theta$ distribution—along ϵ_D: The polarized laser photoselects molecules for dissociation. Because the μ's are preferentially along Z, the H_2O planes are aligned preferentially about the X, Y plane.

One of the H_2O planes is shown at the bottom of Fig. 4 in order to discuss the dissociation which occurs after absorption of the 157 nm photon. It shows the H_2O molecule together with the products H and OH and their linear momenta $\mathbf{p}_H$ and $\mathbf{p}_{OH}$.

For the internally cold H_2O molecules which constitute the nozzle beam, rotation can be neglected to a first approximation. In this case the OH product will rotate after the dissociation in the original H_2O plane because all the forces during the dissociation act in that plane. The classical angular momentum J_{OH} will be perpendicular to the original H_2O plane and thus have the same $\cos^2 \theta$ distribution as the photoselected transition moments μ of H_2O. The idealized fragmentation discussed above corresponds to a completely planar dissociation process which is realized only for internally cold H_2O.

Returning to the upper part of Fig. 4 we discuss the subsequent absorption of the linearly polarized probe laser by the aligned OH molecules. We use only Q lines for the excitation of OH because for these lines the transition moment μ_E for the absorption is perpendicular to the OH rotation plane (which is the original H_2O plane).[14] Thus μ_E will have the same $\cos^2 \theta$ distribution as J_{OH}: The μ_E are preferentially aligned along Z.

We consider now the two cases where the electric vector ϵ_E of the probe laser is along Z ($\|\epsilon_D$) or along Y ($\perp\epsilon_D$). The excitation probability of OH, given by $|\epsilon_E \cdot \mu_E|^2$, depends strongly upon ϵ_E: If ϵ_E is along Z maximum excitation occurs because the μ_E are preferentially aligned along Z. Correspondingly, $\epsilon_E \perp \epsilon_D$ gives minimum excitation. Neglecting finer details about the fluorescence anisotropy (which will be discussed later) we see immediately that for $\epsilon_E \| \epsilon_D$ more fluoresence will be observed by the photomultiplier than with $\epsilon_E \perp \epsilon_D$. With an appropriate analysis, which includes also deviations from planar dissociation, the quantitative spatial alignment of OH can be extracted from the measurement of the fluorescence intensities for $\epsilon_E \| \epsilon_D$ and $\epsilon_E \perp \epsilon_D$.

Even in the case of a completely planar dissociation, it will be shown that the polarization shows a strong J_{OH} dependence which is explained by both hyperfine interaction and Λ-doublet mixing.

III. EXPERIMENTAL

The technique of laser-induced fluorescence (LIF) is well known,[15] so only a brief description of the apparatus will be given. Two antiparallel laser beams are directed to be horizontal and coaxial. The first of these is an excimer laser at 157 nm which dissociates H_2O. The second, which probes the nascent OH via LIF, is a Nd:YAG pumped dye laser operated here in the 306–320 nm range to excite OH transitions. Fluorescence light is then collected as a function of the dye laser wavelength. For low dye-laser power, the relative populations $n(v'', J'')$ in the $^2\Pi_i$ state of OH can be calculated from the fluorescence intensity I of the $^2\Sigma^+, v', J' \rightarrow X\,^2\Pi_i, v'', J''$ transition using the relation

$$n(J'', v'') \propto I/(BP) \quad \text{(linear regime)}, \tag{1}$$

where B is the tabulated Einstein transition probability for the absorption[16] (proportional to the product of Hönl–London and Franck–Condon factors) and P is the laser power. If the laser power is sufficiently strong to saturate all transitions (our most usual operating mode), the population is directly proportional to the fluorescence intensity, independent of laser power or transition probabilities:

$$n(J'', v'') \propto I \quad \text{(saturation)}. \tag{2}$$

Equations (1) and (2) also hold for spin and Λ-doublet sublevels. A complication arises only if satellite line overlap occurs, because then we saturate a three level system.

We present here a brief review of the spectroscopy of OH in order to avoid later confusion. For the most part, we follow the classic work of Dieke and Crosswhite (DC),[17] who used the notation of Hund's case (b). Case (b) assumes that the spin is coupled to the rotation rather than to the internuclear axis. In this scheme the total angular momentum J_{OH} is expressed as $N + 1/2$ and $N - 1/2$ for the $\Pi_{3/2}$ and $\Pi_{1/2}$ states, respectively, where N is the total angular momentum quantum number without spin: i.e., the resultant of the angular momentum O of the rotating nuclei and the electronic angular momentum L. DC used K instead of N, otherwise we retain their notation.

The energy diagram for several rotational states of the $^2\Sigma^+ - ^2\Pi_i$ transition is shown in Fig. 5, which is adapted from Ref. 18. The selection rules for this transition are $\Delta J = 0, \pm 1$ and $+ \leftrightarrow -$. For case (b) coupling there is the additional rule that $\Delta N = 0, \pm 1$, where $\Delta N = N' - N''$. Lines satisfying both selection rules constitute main branches. Transitions which violate the ΔN rule are the satellite

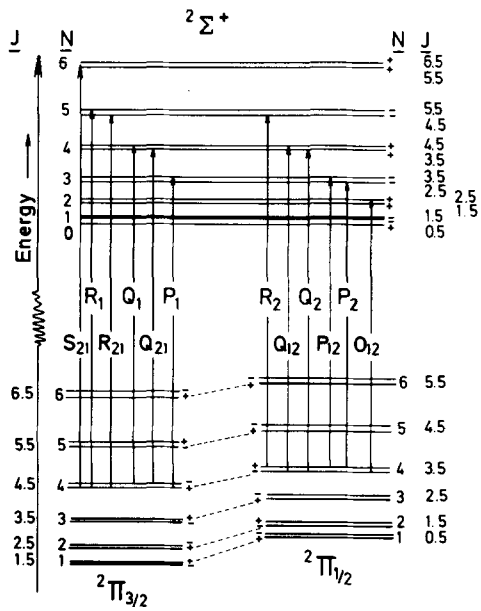

FIG. 5. Energy level diagram of OH, which is not to scale. This serves to explain notation (see the text).

branches. For large values of N, where case (b) is a good approximation, the satellite intensities are negligible compared to the main line intensities, whereas at low values of N the intensities are comparable. DC label main branches as P, Q, or R depending on whether ΔN changes by 1, 0, or -1, respectively, with a single subscript 1 or 2 referring to the $\Pi_{3/2}$ or $\Pi_{1/2}$ states, respectively. Therefore, the main branches have $\Delta J = \Delta N$ and reference to either J or N can be used to designate a given branch. This is not true for the satellite lines, and we will subsequently need to work with changes in J rather than N. For example, the DC satellite P_{12} really belongs, in terms of ΔJ, to the Q branch. A line designated $P_2^0 4$, for example means $\Delta N = -1$, $v'' = 0$, belongs to the $\Pi_{1/2}$ state and has $N'' = 4$.

The spectroscopic assignments[17–19] of the upper and lower Λ doublet are unambiguous, and parity selection rules show that P and R lines probe Π^+ and Q lines probe Π^- levels. However, the direction of the $p\pi$ lobe with respect to J has been controversial: basically the question has been whether a $p\pi^3$ hole behaves differently from a $p\pi^1$ electron. We will subsequently discuss this point. However the above consideration and our experiment indicate that the correct assignments (at high J) are as given in Fig. 2.

A. Apparatus

The reaction vessel was a stainless steel chamber equipped with baffled arms to reduce scattered light from the two lasers. The chamber was evacuated with two 10 in. oil diffusion pumps, which produce a base pressure less than 10^{-6} Torr. The apparatus, as used for experiments with polarized light, is shown in Fig. 6. For the other measurements the polarizers and $\lambda/2$ plate are removed and Brewster windows are substituted for those shown.

Distilled water was introduced to the chamber by three different methods in order to study the influence of initial H_2O rotation prior to dissociation. These were (a) as a nozzle beam, (b) as an effusive beam, and (c) as vapor.

A cold beam of H_2O was produced by bubbling argon through water (30 Torr Ar/18 Torr H_2O) and expanding the mixture through a pulsed nozzle. The pulsed source was a commercial fuel injection valve (Bosch) modified to give a short open time by (a) using a stiffer spring, (b) changing the coil of the solenoid, (c) using a short current pulse (shorter than the actual open time) to accelerate the active bar, and (d) moving the gas inlet to be near the nozzle. The performance of the resulting molecular beam could be monitored by directing it through an open ion gauge. The final pulse length was adjustable from 250 to 1000 μs. The active bar bounced at the end of the pulse but this was unimportant since the measurements were done before that time. Source conditions were adjusted ($d \sim 1$ mm, $P_0 \sim 50$ Torr) to maximize cooling of the water [$\propto (P_0 \cdot d)^{1/2}$] with a minimum of dimerization ($\propto P_0/d$).[20] The beam was analyzed with a quadrupole mass spectrometer located down stream and no water clusters were observed. This is reasonable since others[21] have reported only a few percent of $(H_2O)_n$.

An estimate of the rotational temperature in the nozzle beam was made by adding a small amount of NO to the source gas and measuring (by LIF) its rotational temperature. This was 10 K which should be close to the rotational temperature of the water. Accordingly nearly all of the H_2O molecules are in their rotational ground state. Due to the conservation of nuclear spin during the relaxation, some H_2O molecules have to end up in $J = 1$ states. Unfortunately we can not measure the rotational distribution of H_2O molecules directly, but our experimental data indicate that most H_2O molecules should be in the rotational ground state. The nozzle was 1 cm from the interaction region. The excimer was fired so as to photolyze water only in the center of the gas pulse, where maximum cooling occurs.[22]

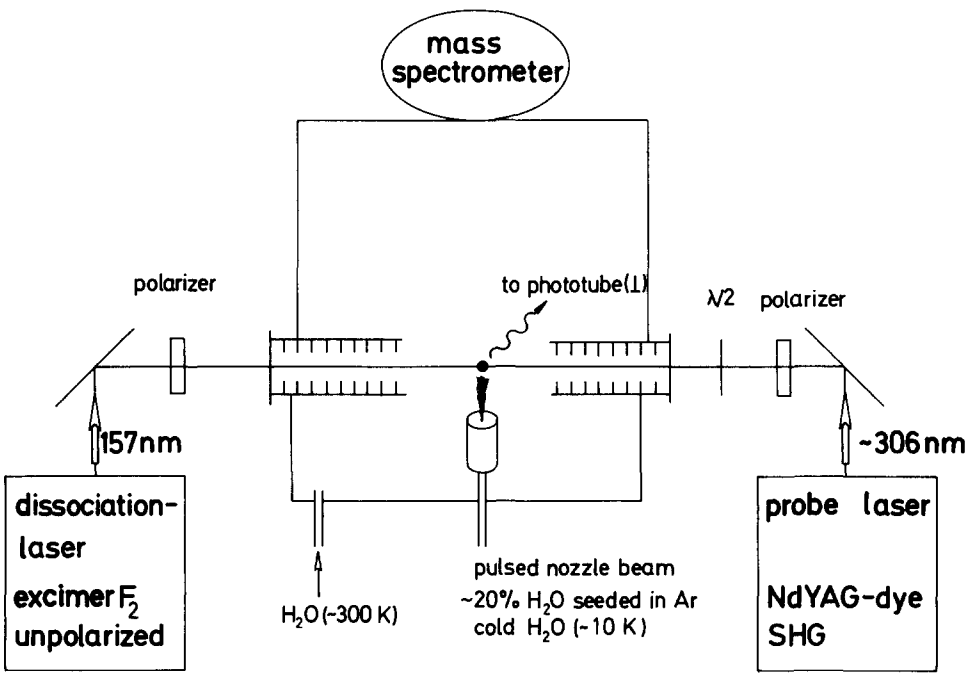

FIG. 6. Experimental configuration.

Higher temperature water was studied with the use of a continuous effusive flow source, i.e., a 1/4 in. copper pipe pointing near the interaction region. Obviously we obtain some rotational cooling of the H_2O molecules and it might be that we do not have a true effusive, but a slightly sonic beam under these conditions. This should be kept in mind for the remaining part of the paper. The H_2O pressure in the chamber was then maintained at $\sim 3\times 10^{-5}$ Torr although the local H_2O density at the interaction region was somewhat higher. A nearby LN_2 trap served as a cryopump. Because some water could reflect from this cold surface and then be photolyzed, the internal energy of H_2O might be lower than room temperature. This was again checked with NO which was bubbled through the water under similar conditions. Its rotational temperature was ~ 260 K, independent of the presence of LN_2 in the trap. This slight cooling may result from expansion of the gas through the leak valve. We believe that the rotational temperature of H_2O in the effusive beam is lower than 260 K, based on the rotational distributions presented later.

Finally, water of room temperature was studied using a flow system, as described previously.[23] In this case, there were no cold traps and the inlet line was sufficiently large to insure the water was truly thermalized at 300 K.

The photolysis light was the 157 nm line of a Lambda Physik EMG 200 excimer laser, which delivers ~ 15 mJ/pulse in about 12 ns. The laser operated at 10 Hz. The rapidly diverging VUV beam was focused into the cell with two CaF_2 lenses through a CaF_2 window. At the interaction region the beam is rectangular and matches the molecular beam profile. The light path was flushed with dry Ar to prevent absorption of the VUV by air. The useful lifetime of the excimer's gas mixture (0.17% F_2, 9.4% Ne, 90.4% He) was only about 15 min and the data were corrected for the power decrease with time.

The probe laser was a frequency doubled Nd:YAG pumped dye laser (Quantel TD1 III system). The dye laser output at the desired UV wavelengths was 2 mJ and was sufficient to saturate all transitions measured, so that Eq. (2) could be used. However low power measurements analyzed with Eq. (1) gave the same results.

Firing of the lasers was governed by a central clock which sent one pulse to the pockets cell of the YAG, and another to trigger the excimer laser. The delay between photolysis and probe light was variable from 0 to 1 ms. A delay of 100 ns is adequate to give nascent distributions of OH and to avoid electrical noise and scattered light. The clock also actuated the pulsed nozzle source.

Fluorescence from a small solid angle, which was perpendicular to the laser beams, was collected by imaging optics (quartz) and viewed by a cooled RCA 31034 PMT which was typically operated at 1600 V. The scattered VUV light is removed by a Schott color filter (UG 11). The PMT signal was measured either as (a) a current, with an electrometer, or (b) a voltage, with a PAR 162/165 Boxcar integrator.

For the polarization experiments both lasers were linearly polarized. The light emerging from the excimer is unpolarized. It is passed through a MgF_2 Rochon prism (B. Halle, Berlin) which yields fully linearly polarized light at its exit. The direction of the electric vector of the dissociation light ϵ_D can be adjusted to any desired angle by turning the Rochon.

The dye-laser light is initially linearly polarized. However, because there is some subsequent depolarization by mirrors, we insert a Glan–Thompson prism so that the light is fully linearly polarized. The light is then directed through a $\lambda/2$ plate so that the probe laser's electric vector ϵ_E can be adjusted to any desired angle.

Brewster windows were normally used to introduce the laser light to the apparatus. For the polarization experiments, they were replaced by windows normal to the laser rays, as shown in Fig. 6.

B. Data collection and analysis

1. Distribution measurements

In order to measure the various distributions (vibrational, rotational, fine structure, and Λ doublets), the data collection and its subsequent normalization had to be carefully performed. Because the relevant lines are found in a wide range of wavelength, scans of the entire spectral range were impractical because of the rapid decay of the excimer laser. By observing the fluorescence from a single rotational line for the life of the excimer's gas mixture (~ 15 min), it was found that, after an initial exponential decay (~ 2 min), the intensity decreased linearly with time. Therefore the following procedure was used.

For a given $(^2\Pi_i, v'')$, the distribution of N'' was obtained by measuring the intensity of the $N''=4$ line of the Q or R branch in question at the beginning and the end of the linear portion of the gas fill. The other N'' lines (of the same branch) were then measured in the interval between. These intensities were normalized to that of the $N''=4$ found by the linear relationship. For example, to find the distribution in R_1N'' of the $^2\Pi_{3/2}, v''=0$ state, the N'' sequence 4, 3, 2, 1, 4 was measured. $R_1 3$ was then divided by the value which $R_1 4$ would have had at that time, and so on for $R_1 2$, and $R_1 1$.

To obtain the *relative* populations in the $v''=0$ and $v''=1$ states the ratios $Q_i^0 4/Q_i^1 4$ and $R_i^0 4/R_i^1 4$ were sequentially measured, where the superscripts are the values of v''. Similarly, to obtain the *relative* populations in the $^2\Pi_{3/2}$ to $^2\Pi_{1/2}$ states the ratios $Q_1 4/Q_2 4$ and $R_1 4/R_2 4$ were determined, and to find the relative populations in the Λ doublets the ratios $Q_i 4/R_i 4$ were directly measured. The unexpected large differences in the populations of the Λ doublets obtained by the normalization procedure led us to verify the results by directly measuring the ratios Q_iN''/R_iN'' for many values of N''. These Λ doublet results were also substantiated by measuring the Q_iN''/P_iN'' ratios for several lines. These apparently redundant procedures were necessary because of the rapid decay of the excimer's power.

The effusive beam, nozzle beam, and cell distributions were measured independently. A *direct* comparison of nozzle and effusive beams measurements were also made, particularly for the Λ-doublet populations, which showed a dramatic difference at different internal temperatures of the water (see below). It was possible to measure (for the same excimer laser fill) intensity ratios for Q_1N''/R_1N'' for effusive and nozzle beams. These could be quickly interchanged so

that the comparison was quite precise. That these ratios differed is only due to the internal temperature of the water, since all other conditions of laser alignment, excimer power, etc. were the same.

2. Polarization measurements

a. Data acquisition. The setup and the basic principle of the polarization experiment were discussed in Sec. II, and illustrated in Fig. 4, and are not repeated here.

Although we can arbitrarily select the directions of the electric vectors of both dissociation and probe lasers, we use only two directions: ϵ_D and ϵ_E are either along Z or along Y. This gives the four possible cases:

$$\text{(a)}\,\epsilon_E \| \epsilon_D \| Z; \quad \text{(b)}\,\epsilon_E \perp \epsilon_D \| Z;$$

$$\text{(a')}\,\epsilon_E \| \epsilon_D \| Y; \text{(b')}\,\epsilon_E \perp \epsilon_D \| Y.$$

For most of our data we used $\epsilon_D \| Z$ and measured the fluorescence intensity I at the phototube for both $\epsilon_E \| \epsilon_D$ and $\epsilon_E \perp \epsilon_D$. We define the polarization ratio R as

$$R \equiv \frac{I(\epsilon_E \| \epsilon_D \| Z)}{I(\epsilon_E \perp \epsilon_D \| Z)} = \frac{\text{case (a)}}{\text{case (b)}}. \tag{3}$$

This polarization ratio is measured for the different rotational states of OH in both $v'' = 0$ and $v'' = 1$. We use only Q lines for the excitation of OH because they give larger polarization effects. The typical experimental procedure was the following.

The polarizing optics are adjusted, for example, for case (a). The intensity of the LIF is measured on a strip chart recorder for about a minute. The direction of ϵ_E is then turned 90° to yield case (b) and the new LIF intensity is measured. This procedure is repeated several times. Because the measurements only involved the relative fluorescence intensities of a given rotation-vibration state at two positions of the ϵ vectors, the correction for the decrease in excimer power was small. This procedure was repeated for all resolved Q_i lines.

We also performed measurements with directions of ϵ_D and ϵ_E according to case (a') and (b') to check the measured polarization ratio. With the appropriate analysis we find consistent results.

To compare the polarization for the H_2O from either nozzle or effusive beam we just turn the nozzle beam off and the effusive beam on. In this way we replace the water probe without changing the experimental setup. This was done quickly and gave an accurate relative measurement for the dissociation from rotationally cold and warm H_2O. No polarization data were obtained with 300 K H_2O.

For the polarization experiments, the dye-laser power had to be reduced by a factor of 100 to avoid saturation effects. Further reduction did not influence the measured polarization effect, which indicated that the experiments were performed in the linear regime. We also directly observed the fluorescence intensity to be linear with dye laser power.

The ratio of fluorescence intensity at two polarizer settings was sensitive to the base line, which depends on scattered light. We therefore measured the base line with both lasers on but the water source off. Base line checks were also made for each configuration of the ϵ vectors to avoid any changes in detected signal due to polarization dependent background. Similarly comparisons could be made with the dye laser detuned from the transitions.

The polarization ratios were reduced by magnetic fields greater than ~ 3 G, and we took care to show that those fields present (such as those of the nozzle source solenoid and that of the earth) did not influence the measurement.

b. Analysis of polarization data. The polarization data are analyzed for alignment of J_{OH} with the use of a classical dipole model, which we present below. We do so because (a) the basic ideas are easier to understand, (b) the classical model is more easily modified to include an additional feature needed here, and (c) comparison with the recent quantum calculations of Greene and Zare (GZ)[24] shows that the quantum correction for the case of OH is well below those in the experiment.

We previously presented the appropriate data reduction formulas, which were derived from a similar approach used earlier.[25,26] The results are, in the high-J limit, identical to those derived by GZ in their quantum calculations.

In our LIF excitation, charge is moved from a $p\sigma$ orbital which is parallel to the OH axis to a $p\pi$ orbital perpendicular to it, i.e., a Σ–Π transition. This clearly requires a transition moment (μ_{OH}) which is perpendicular to the internuclear axis. However, this subdivides, in the high J limit, into the cases in which the $p\pi$ lobe, and thus μ_{OH}, is either perpendicular or parallel to J_{OH}.

Case, McClelland, and Herschbach[14] found for high J and for linearly polarized light, that $|\epsilon_E \cdot \mu_{OH}|^2$ is equal to $|J_{OH} \cdot \epsilon_E|^2$ for Q transitions and to $\frac{1}{2} - (J_{OH} \cdot \epsilon_E)^2/2$ for P or R transitions. This result corresponds to the well-established interpretation that μ_{OH} lies along J_{OH} for Q transitions, but rotates in the plane of rotation (POR) for P or R transitions.[25] In this section the Q, R, and P branches refer to ΔJ, not to ΔN. Stronger polarization occurs with Q lines, because here μ_{OH} remains fixed in space. Accordingly we chose to use Q excitations for our polarizaton measurements.

We describe the data analysis with the aid of Fig. 7, which defines the important angles and coordinates for the classical dipole model.

If the detector is along Y we have the same system as in Fig. 4, where ϵ_D and J_{OH} define the angle θ. This corresponds to the cases (a) and (b) with ϵ_D along Z. However, for cases (a') and (b'), where ϵ_D is along Y, we could redefine angles. Instead of doing this, we allow ϵ_D to remain along Z, but we move the detector to the Z direction. Because this corresponds only to a permutation of the Y and Z axis we obtain the same result as if both ϵ_D and the detector are along Y.

We now proceed to find a joint probability of (a) exciting and dissociating H_2O so that J_{OH} has a particular orientation (b) of exciting that OH with a Q transition and (c) finding the component of each (P, Q, or R) emission dipole on a particular cartesian axis. The total fluorescence emitted along X, Y, or Z is the sum of the emission dipole components along the two normal axes.[25]

(a) We previously stated that the distribution of J_{OH} should have a $\cos^2\theta$ distribution. However because that was

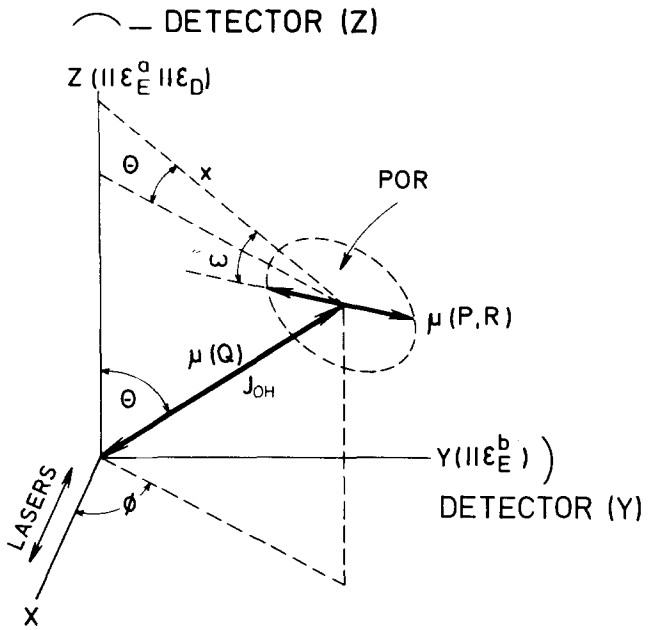

FIG. 7. Schematic of polarization analysis. Shown are laboratory coordinate X, Y, and Z, and molecular coordinates. This serves to illustrate the classical model for polarization (see the text). The abbreviation POR means plane of rotation.

an idealized limit for a completely planar dissociation process, we use instead a more general distribution of J_{OH} vectors

$$W(J_{OH}) = 1 + \beta P_2(\cos\theta),$$
$$\text{with } P_2(\cos\theta) = \tfrac{1}{2}(3\cos^2\theta - 1), \quad (4)$$

where P_2 is the second Legendre polynomial and β is an anisotropy parameter. This reduces to the previous $\cos^2\theta$ distribution used in Sec. II when $\beta = 2$, and to an isotropic distribution for $\beta = 0$. Thus the probability of creating an OH with an angle θ is given by $(k_D I_D/3)[1 + \beta P_2(\cos\theta)]$, where k_D is a constant, I_D is the dissociation laser intensity, and the factor 3 helps in comparison with calculations in which a $\cos^2\theta$ distribution is used.

(b) Figure 7 shows a direction of J_{OH}, which is described by the angles θ and ϕ, as well as the POR of the OH, which is perpendicular to J_{OH}. All our analyzed results use Q branch laser excitation (i.e., $\Delta J = 0$). In this case μ_{OH} lies, in the high-J limit, along J_{OH} and the angle-dependent OH excitation probabilities are $k_E I_E \cos^2\theta$ and $k_E I_E \sin^2\theta\sin^2\phi$ for cases (a) and (b) respectively. Again k_E is a constant, I_E is the intensity of the probe laser, and the trigonometric factors are those for the squares of the projections of μ_E on the Z and Y axes, respectively.

(c) Now we consider the fluorescence from the laser-excited OH molecules. This is emitted as unresolved P, Q, and R lines. Because the P and R lines emit radiation with the same angular dependence and because Q has a different dependence, we treat these two cases separately and finally add their separate contributions. We proceed by finding the components of the emission transition moment μ_{em} along the three Cartesian axes. For the Q lines, the transition moment for emission has the same direction as that for excitation, i.e., $\mu_E \| \mu_{em}$. Thus the component in the Z direction is $k_{em} I_{em} \cos^2\theta$, where k_{em} is a constant and I_{em} is the total emission. The analogous trigonometric factors are $\sin^2\theta\sin^2\phi$ and $\sin^2\theta\cos^2\phi$ for the Y and X axes, respectively.

The P and R fluorescence is more complicated, and less polarized, because in these cases μ_{em} is not fixed, but rotates in the POR. The molecular coordinate system defines a direction x as that of the intersection of the POR and the J_{OH}-Z plane, and ω is the angle, in the POR between μ_{em} and x. By the consideration of a molecular axis y (not shown in the already busy Fig. 7), which is perpendicular to x in the POR, we may find the projection of μ_{em} on the three axes. The trigonometric factors are $\sin^2\theta\cos^2\omega$, $(\cos\omega\cos\theta\sin\phi + \cos\phi\sin\omega)^2$, and $(\cos\omega\cos\theta\cos\phi - \sin\phi\sin\omega)^2$ for the Z, Y, and X axes respectively.

The previously discussed joint probability is now integrated over the solid angle $\sin\theta\, d\theta\, d\phi$. The integrals are normalized by dividing by 4π for double integrals, and by $8\pi^2$ for triple integrals, (i.e., those involving ω). As an example consider, for case (b) the component of the emission dipole upon the Z axis I_Z in the emission of a P line. The overall probability is

$$K/(3\cdot 8\pi^2)\int_0^{2\Pi}\int_0^{2\Pi}\int_0^{\Pi}[1 + 1/2\beta(3\cos^2\theta - 1)]$$

dissociation

$$\times \sin^2\theta\sin^2\phi\sin^2\theta\cos^2\omega\sin\theta\, d\theta\, d\phi\, d\omega,$$

absorption emission

where $K = k_D I_D k_E I_E k_{em} I_{em}$, and the result is $K(2/45)(1 - 2\beta/7)$.

The results for all 12 cases are shown in Table I. Also shown there are the weighted sums of the actual emission intensities which consist of one part Q emission and 1/2 part each of P and R emission. These weights are in accord with observations.

The fluorescence observed at the Z detector is proportional to $I_X + I_Y$, while that at the Y detector is proportional to $I_X + I_Z$. (This analysis could also be applied to observations of the degree of polarization, where, e.g., a polarization filter at Y would measure I_Z/I_X.) We find that for our four cases the intensities are:

TABLE I. The components of the emission transition moment on the three Cartesian axes for cases (a) and (b) for which $\epsilon_E \| \epsilon_D$, and $\epsilon_E \perp \epsilon_D$, respectively for (1) a Q excitation and a Q emission ($Q\uparrow Q\downarrow$) and (2) a Q excitation and a P (or R) emission ($Q\uparrow P\downarrow$). Also shown are the weighted sums for our case, i.e., Q emission represents 1/2 of total emission. Units are in $K/45$, where K is defined in the text.

Component	Case (a)	Case (b)	Transition
I_Z	$3(1 + 4\beta/7)$	$1 + \beta/7$	$Q\uparrow Q\downarrow$
I_X	$1 + \beta/7$	$1 - 2\beta/7$	$Q\uparrow Q\downarrow$
I_Y	$1 + \beta/7$	$3(1 - 2\beta/7)$	$Q\uparrow Q\downarrow$
I_Z	$1 + \beta/7$	$2(1 - 2\beta/7)$	$Q\uparrow P\downarrow$(or $Q\uparrow R\downarrow$)
I_X	$2(1 + 13\beta/28)$	$2(1 - 5\beta/28)$	$Q\uparrow P\downarrow$(or $Q\uparrow R\downarrow$)
I_Y	$2(1 + 13\beta/28)$	$1 - \beta/14$	$Q\uparrow P\downarrow$(or $Q\uparrow R\downarrow$)
	Weighted sums		
I_Z	$4(1 + 13\beta/28)$	$3(1 - \beta/7)$	$(Q\uparrow Q\downarrow + Q\uparrow P\downarrow)$
I_X	$3(1 + 5\beta/14)$	$3(1 - 3\beta/14)$	$(Q\uparrow Q\downarrow + Q\uparrow P\downarrow)$
I_Y	$3(1 + 5\beta/14)$	$4(1 - 13\beta/56)$	$(Q\uparrow Q\downarrow + Q\uparrow P\downarrow)$

$$\text{(a) } 7+41\beta/14, \quad \text{(b) } 6-15\beta/14, \tag{5}$$

$$\text{(a') } 6+15\beta/7, \quad \text{and} \quad \text{(b') } 7-11\beta/7,$$

so that the polarization ratio [Eq. (3)] is

$$R=\frac{7+41\beta/14}{6-15\beta/14}. \tag{6}$$

Note, that even for an isotropic distribution of OH ($\beta=0$), which corresponds to the completely depolarized case, the polarization ratio is larger than one ($R=7/6$). This is because, with Q excitation, the Q emission lines have a higher degree of polarization than do the P or R lines, since in the former case μ_{em}, remains fixed in space.

Formula (6) may be inverted so as to determine the anisotropy parameter β from the measured polarization ratio R,

$$\beta=\frac{84R-98}{15R-41}. \tag{7}$$

With the detector at Z, we can also define another polarization ratio R' which corresponds experimentally to the cases (a') and (b') with ϵ_D along Y. In this case we obtain

$$R'=\frac{6+15\beta/7}{7-11\beta/7} \quad \text{and} \quad \beta=\frac{49R'-42}{11R'+15}.$$

In addition other ratios could be taken, like case (a)/case (a') and used as an additional check for the measured polarization. The ability to determine β by making independent measurements of both R and R' yields added confidence that the data are not influenced by spatial anisotropies such as might be caused by the direction of the molecular beam, stray magnetic fields, or polarization dependent transmissions at windows or photomultiplier.

The main approximation in this classical model is the assumption of the high-J limit, with J_{OH} perpendicular to the OH rotation plane and the transition moments either perpendicular (Q lines) or parallel (P, R lines) to the rotation plane. At lower J_{OH}, which are important here, this approximation breaks down.

In the quantum treatment of this problem by GZ[24] these effects are included (although they still neglect Λ-doublet mixing). They find that the fluorescence intensities can be written as a sum of products of molecular alignment parameters $A_0^{(2)}$, geometrical factors in excitation and detection k, and angular momentum coupling factors ω. The k are tabulated by GZ. We evaluated the ω, which involve Wigner $6j$ and $9j$ symbols, for Q excitation and the results are in Table II. Our arrangement is called the mutually orthogonal geometry by GZ, and our case (a)/case (b), is equal to their (case 1 + case 2)/(case 3 + case 4).

The molecular alignment parameter $A_0^{(2)}$ is related to the high-J limit to our anisotropy parameter β by

$$A_0^{(2)}=\tfrac{2}{5}\beta. \tag{8}$$

It can be shown via Eq. (25) of Ref. 27, that for $\beta=2$, which is the value found by us for cold H_2O,

$$A_0^{(2)}=0.8-\frac{3}{5J(J+1)}.$$

Our calculations show that the difference between our classical values for OH, and those of GZ, are fractions of a percent and far less than our experimental precision. As will be shown later, depolarization due to hyperfine structure, also treated by GZ, is more significant here.

IV. RESULTS

A. State distributions of OH photolyzed from 300 K water

In the distribution measurements, in contrast to the polarization measurement, the power of the probe laser was kept sufficiently high to saturate *all* the transitions. Therefore, the fluorescence intensity for a given transition is directly proportional to the population in the lower state.

1. Rotational distribution

Measured rotational distributions of OH($^2\Pi_i, v''=0, 1$) are represented by Boltzmann plots in Fig. 8. Several features will be pointed out here and discussed in more detail in Sec. V.

Consider the OH($v''=0$) distribution first. The data of Fig. 8, for 300 K H_2O, agree with our earlier results for $v''=0$.[23] There is still curvature at low angular momenta, although particular care was taken to insure that collisional relaxation was not involved. After the first few rotational states, the distributions for both spin states lie on a straight line corresponding to an effective rotational temperature of 930 K.

Similar behavior is also observed in the rotational distribution of the $v''=1$ state: curvature at low N'' followed by approximately linear behavior at higher values. The rotational temperature is 840 K. The 90 K "temperature" difference in the rotational distributions of the two vibrational states is significant.

Because of predissociation, only the first few rotational states in $v''=2$ could be measured, so a full distribution is not shown here. Nevertheless the first few data points, for $N''=1$–4, indicate that the rotational temperature is not drastically different.

TABLE II. Greene–Zare functions $\omega(k_d, k_a, k, J_i, J_e, J_f)$. All values should be divided by $3(2J+1)^2$. They are for Q-branch excitation only, i.e., $J_i=J_e=J$.

k_d, k_a, k	$J_f=J$	$J_f=J+1$	$J_f=J-1$
0, 0, 0	1	1	1
2, 2, 0	$(2J+3)(2J-1)/[\sqrt{20}J(J+1)]$	$-(2J-1)/[\sqrt{20}(J+1)]$	$-(2J+3)/[\sqrt{20}J]$
2, 0, 2	$[-J(J+1)-3]/\sqrt{2}J(J+1)]$	$[J(J+1)-3]/[\sqrt{2}(2J+3)(J+1)]$	$[J(J+1)-3]/[\sqrt{2}J(2J-1)]$
0, 2, ,2	$-1/\sqrt{2}$	$-1/\sqrt{2}$	$-1/\sqrt{2}$
2, 2, 2	$-(2J^2+2J+3)/[\sqrt{14}J(J+1)]$	$(2J^2+2J+3)/[\sqrt{14}(J+1)(2J+3)]$	$(2J^2+2J+3)/[\sqrt{14}J(2J-1)]$

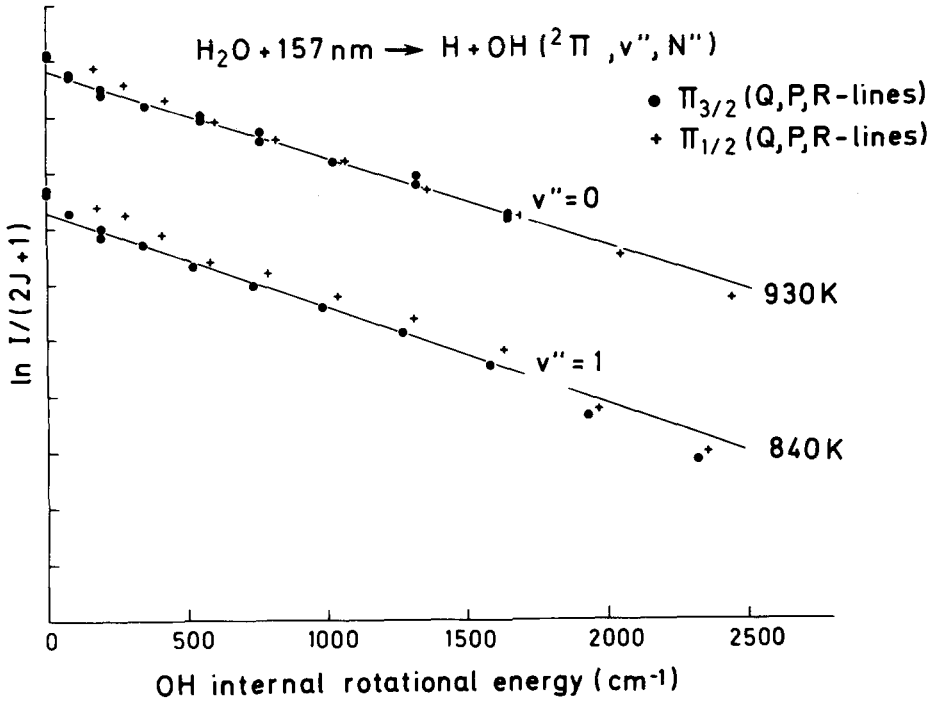

FIG. 8. Boltzmann plot of the rotational distributions of the OH fragments formed in the photolysis of 300 K water for both $v'' = 0$ and $v'' = 1$. Different symbols are used for the two spin states. The numbers at the right are the rotational temperatures corresponding to the straight lines. For clarity the two curves are vertically separated.

2. Vibrational distribution

There is significant vibrational excitation of OH, contrary to an earlier observation[5] and to that expected from simple models for the dissociation process.

The relative populations in two vibrational states v and v' is defined as

$$\frac{n(v)}{n(v')} = \frac{\sum_J n(v,J)}{\sum_J n(v,J)}, \tag{9}$$

where the sums are over all rotational and fine structure states for each vibrational state. Summations over the measured distributions gives $n(v=0)/n(v'=1) = 1.01$. We made several measurements comparing the population in the same rotational state of $v'' = 0$ and $v'' = 1$. For example the ratio of $R_1^0 3/R_1^1 3$ gave a ratio of 0.98.

To check that this ratio has no systematic error which may result from changes in alignment of the probe laser beam (with wavelength change) relative to the spatially sensitive imaging optics, another measurement was made. In this case, the ratio $P_2^0 8/R_2^1 8$ (which are two neighboring lines) was measured several times and gave a value of 1.1. These ratios were used to calculate the relative population of $v'' = 0$ to $v'' = 1$.

In the $v'' = 2$ state we did not measure a full rotational distribution, so that a straight forward evaluation according to Eq. (9) was not possible. To get an estimate of the population in $v'' = 2$ we made line to line comparisons as mentioned before. This gave for $R_1^1 3/R_1^2 3$ the ratio of 6.7. Assuming the same rotational temperature in $v'' = 2$ and $v'' = 1$ this value gives directly the population ratio $n(v''=1)/n(v''=2) = 6.7$.

The above discussion can be summarized by writing the vibrational distribution as

$$n(0):n(1):n(2) = 1.0:(0.96 \pm 0.10):(0.15 \pm 0.05).$$

The higher vibrational states are not accessible via LIF due to predissociation of the $^2\Sigma^+$ state.

3. Spin distribution

The Boltzmann plot in Fig. 8 appears to show that the more energetic $^2\Pi_{1/2}$ spin state has a greater population than the $^2\Pi_{3/2}$ state at small N'' for both $v'' = 0$ and $v'' = 1$. At higher N'', the two spin states converge in the $v'' = 0$ state, while in the $v'' = 1$ the $^2\Pi_{1/2}$ spin population continues to be slightly higher than the $^2\Pi_{3/2}$ spin population. These differences are quite small, as shown in Fig. 9. Here the ratio of the populations in the two spin states, $^2\Pi_{3/2}/^2\Pi_{1/2}$, has been multiplied by the degeneracy, $N/(N+1)$, and is plotted vs the angular momentum N. For a statistical spin distribution, this should be unity for all N. Apparently the $v'' = 0$ vibrational state has a statistical distribution of spin states. The $v'' = 1$ state shows a slight preference for the $^2\Pi_{1/2}$ state.

4. Isotope effect

The photolysis of D_2O was carried out in order to measure the influence of mass upon energy partitioning. Only the rotational distribution for $OD(^2\Pi_i, v'' = 0)$ was measured and the results are shown in Fig. 10. The analogous results for OH are also included for comparison. The OH and OD distributions are very similar. Because the OD has a smaller rotational constant, there is a higher density of points and the curvature at low energy is more apparent. The striking feature of the comparison is the difference in rotational temperatures for the two molecules: D_2O fragmenting to an OD has a narrower rotational distribution than does OH from H_2O. This significant, albeit small, difference is opposite to that expected from a simple impulsive model, which predicts a factor of 4 more rotational excitation in OD

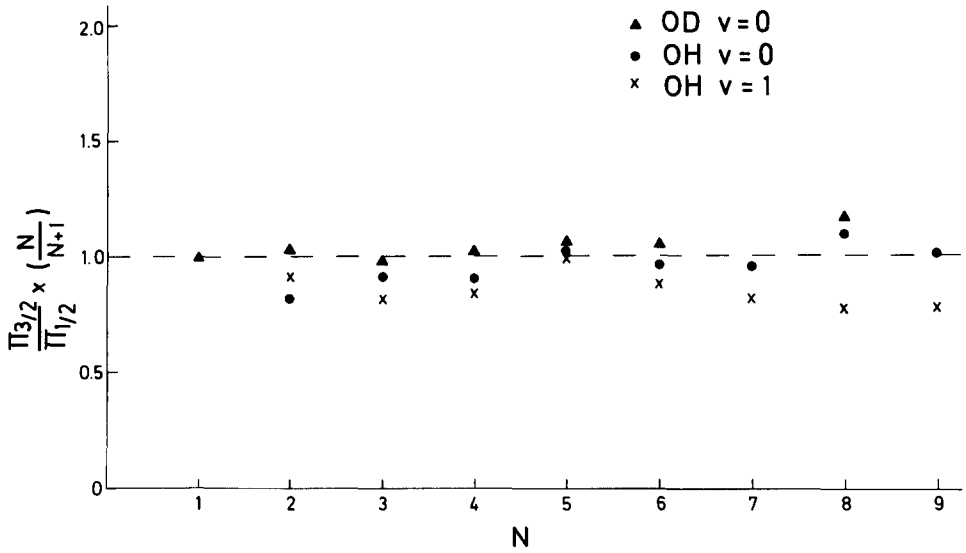

FIG. 9. Ratio of spin populations multiplied by statistical weight as function of N. A value of unity would indicate a statistical distribution.

than in OH. The spin distributions (see Fig. 9) are clearly statistical in OD ($v'' = 0$).

B. Influence of internal temperature of H_2O upon the final state distribution of OH

1. Rotational distribution

Some very interesting and, on first sight, strange effects are seen in the rotational distribution of OH as the H_2O temperature is reduced. These effects are displayed in Fig. 11, which shows the rotational distributions for the $^2\Pi_{3/2}$ spin state of OH ($v'' = 0$ and 1) resulting from H_2O at several internal temperatures. Initially we confine our attention to the left side of Fig. 11, which is for $v'' = 0$. As the H_2O temperature decreases there is a decrease in rotational excitation as is expected if the parents' thermal rotational energy is transferred to the OH. The values are summarized in Table III. Surprisingly, the rotational temperature of the OH radicals is not the same for the distributions measured via the Q and R branches: the R branch is (a) colder and (b) that from 10 K water drastically deviates from Boltzmann behavior, so that the concept of a single rotational temperature is meaningless. For the cold water we obtain a temperature of 210 K for the R branch (see Fig. 11), compared with 930 for the 300 K water. If only initial parent rotation would be transferred to the OH, much less cooling is expected. The difference in the rotational distributions of OH measured via the Q or R branches is actually a measure of the population in the two Λ doublets of OH. The Q branch probes the upper (Π^-) and the R or P branch probes the lower (Π^+) Λ doublet (see Fig. 5).

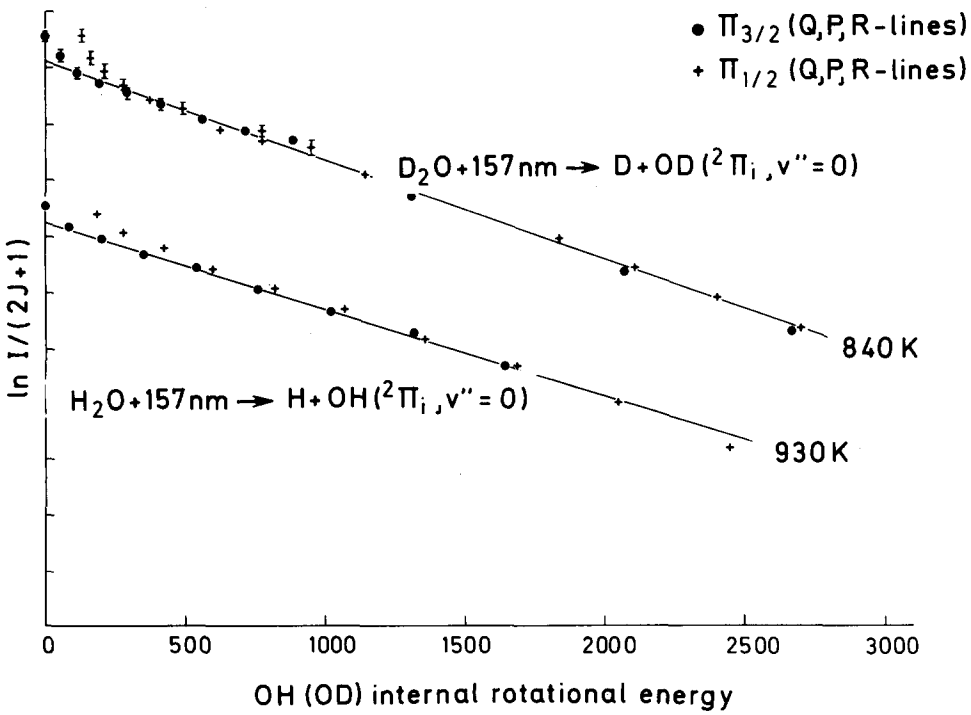

FIG. 10. Isotope effect in the photodissociation of 300 K water. Boltzmann plot of the rotational distribution of OH ($v'' = 0$) and OD ($v'' = 0$) for both spin states. The numbers at the right are the rotational temperatures corresponding to the straight lines. The two curves are arbitrarily displaced vertically.

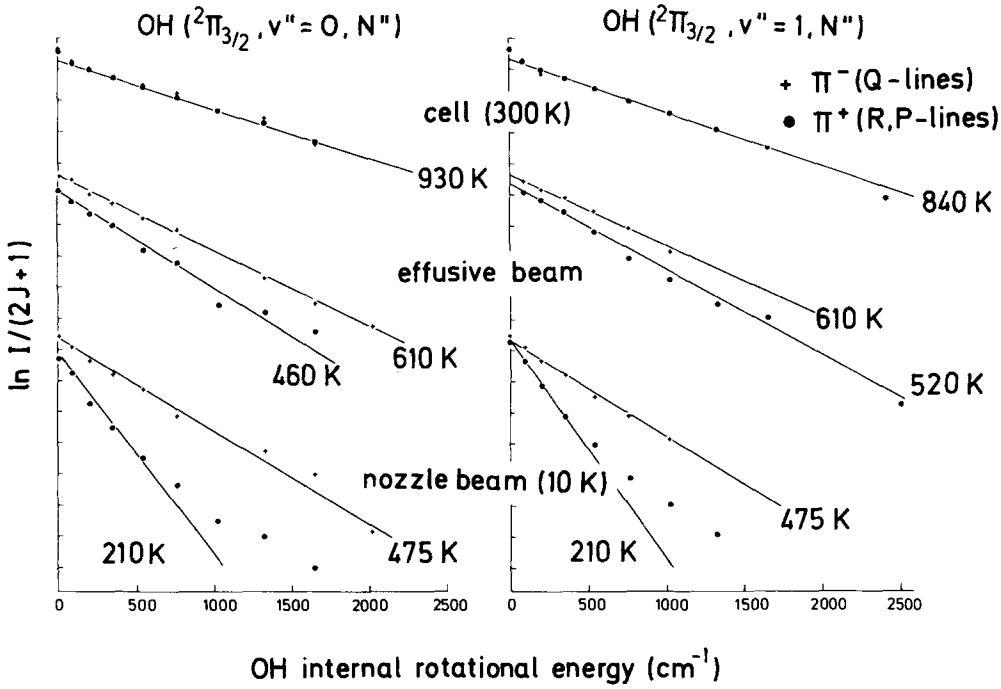

FIG. 11. Influence of initial H_2O rotation on the rotational distributions of OH. The plots on the left are for $v'' = 0$, those on the right are for $v'' = 1$. Only the data for the $^2\Pi_{3/2}$ spin state are shown here. Three different cases, corresponding to different initial rotational temperatures of water (cell, effusive beam, and nozzle beam) are shown. Here the different symbols correspond to the rotational distributions measured via $Q(+)$ and P, R (●) lines. The numbers correspond to the rotational temperature indicated by the straight lines.

This will be discussed later.

The right-hand side of Fig. 11 shows similar behavior for the OH ($v'' = 1$) radicals. For the colder H_2O the OH rotational distribution is the same as that for the $v'' = 0$ vibrational state, within experimental error. (The S/N was worse with the nozzle beam because of lower densities of OH radicals at larger N'').

2. Λ-doublet population inversion

The preferential population in the upper (Π^-) Λ doublet of OH is displayed more clearly in Fig. 12. The original data are those of Fig. 11. Here the fluorescence intensity ratios of Q to R lines represent the population ratios of the Π^- to Π^+ Λ-doublet states. Room temperature water generates statistically populated Λ doublets. Decreasing the water temperature causes an increasing preference for the upper Λ doublet, an effect more strongly exhibited for large N''.

The other spin state, i.e., the $^2\Pi_{1/2}$, showed similar behavior as the $^2\Pi_{3/2}$ state. The low N'' region of $^2\Pi_{1/2}$ could not be studied because of overlap of lines.

That the thermal energy of H_2O plays a role in governing the population of one Λ doublet over another is surprising. The implications of this result will be discussed in Sec. V.

TABLE III. Rotational temperatures[a] of OH (OD) fragments for various internal energies of water. The last column represents the difference between cell and nozzle beam temperature corresponding to a 290 K drop in H_2O temperature.

Product state	Water source: Nozzle beam	Water source: Effusive beam	Cell	ΔT
OH($^2\Pi^+$, $v''=0$)	210 K	460 K	930 K	720
OH($^2\Pi^+$, $v''=1$)	210 K	520 K	840 K	630
OH($^2\Pi^-$, $v''=0$)	475 K	610 K	930 K	455
OH($^2\Pi^-$, $v''=1$)	475 K	610 K	840 K	375
OD($^2\Pi^+$, $v''=0$)	...	...	840 K	
OD($^2\Pi^-$, $v''=0$)	...	...	840 K	

[a] These "temperatures" only approximately describe the data, but serve as an aid in comparing the data (see the text).

C. Polarized laser-induced fluorescence measurement

The measured polarization ratios R are plotted in Fig. 13 as a function of OH angular momentum. The lowest curve is that published previously[28] for water in the effusive beam forming OH($^2\Pi_i$, $v'' = 0$). At that time we thought that the water was 300 K vapor rather than the considerably cooler effusive beam. Also shown in Fig. 13 are the new measurements of R for both $v'' = 0$ and $v'' = 1$ found by photodissociation of water cooled to 10 K. The OH($v'' = 0$) from internally cold H_2O has a higher degree of polarization than the OH($v'' = 0$) from the warm water. This clearly shows the effect of the initial rotation of H_2O on the alignment of OH fragments. The OH($v'' = 1$) from cold water has an even higher degree of polarization than the OH($v'' = 0$). Because of line overlap in the lower N'' of the Q_2 branch, only the Q_1 lines are shown in Fig. 13.

Several observations were made concerning the measured value of R. If the dye power was increased to saturation, the value of R decreased, as expected. If the pressure of H_2O was increased, or if a magnetic field placed near the interaction region, R again decreased. These depolarization effects were studied only to the extent that they could be avoided. To check for possible molecular alignment of H_2O, which might occur in a nozzle beam, several positions of ϵ_D versus ϵ_E were used. With appropriate analysis (see Sec. III B 2) for all different cases we obtain the same alignment parameter β. If the beam molecules were aligned, this would not be true.

The theoretical curves in Fig. 13 are discussed later.

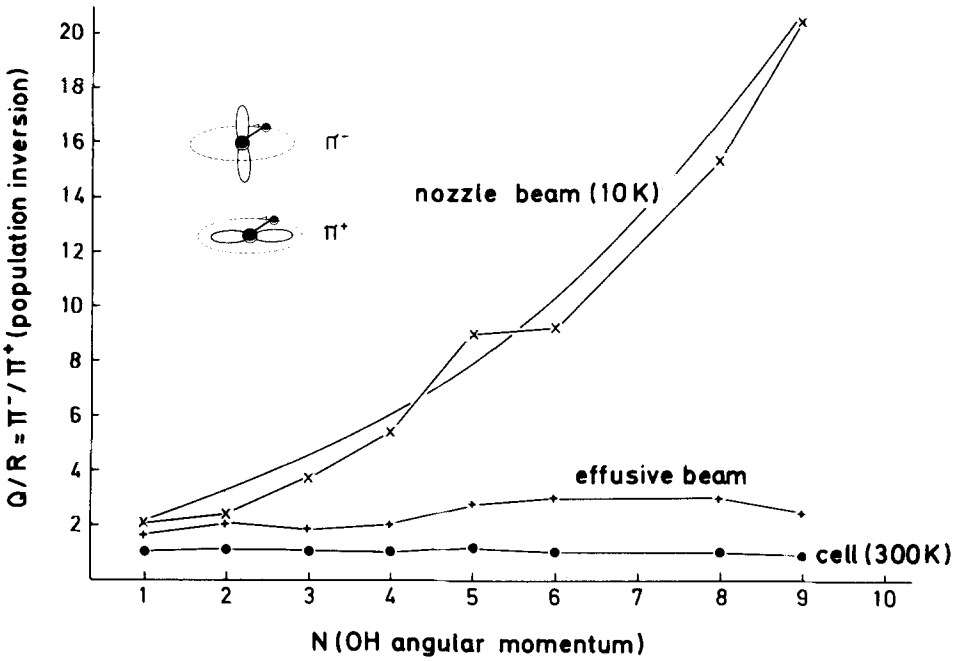

FIG. 12. Population inversion in the Λ doublets. Plotted is the fluorescence intensity ratio of Q vs R lines (taken from Fig. 11), which represents the population inversion in the Λ-doublet states. The three curves differ in the initial rotational temperature of H_2O (nozzle beam, effusive beam, cell). The line without data is from a calculation discussed in the text. The inset shows the electronic configuration for the two Λ doublets.

V. DISCUSSION

A. Energy partitioning

We define the fraction of the available energy (E_{aval}) partitioned into various degrees of freedom as

$$f_R = \overline{E}_R / E_{\text{aval}}, \tag{10a}$$

$$f_V = \overline{E}_V / E_{\text{aval}}, \tag{10b}$$

$$f_T = 1 - f_R - f_V, \tag{10c}$$

where $\overline{E}_R$ and $\overline{E}_V$ are the average rotational and vibrational energies of OH respectively, and

$$E_{\text{aval}} = h\nu + E^P_{\text{int}} - D_0 - [E_v(n) - E_v(0)] \tag{11}$$

is the available energy. The parameters in Eq. (11) are the photon energy ($h\nu = 7.89$ eV), the initial internal energy of the parent $H_2O(E^P_{\text{int}})$, the dissociation energy required to form $H(^2S) + OH(^2\Pi_{3/2}, v'' = 0, N'' = 0)$ from H_2O in its ground electronic, vibrational, and rotational states (D_0),

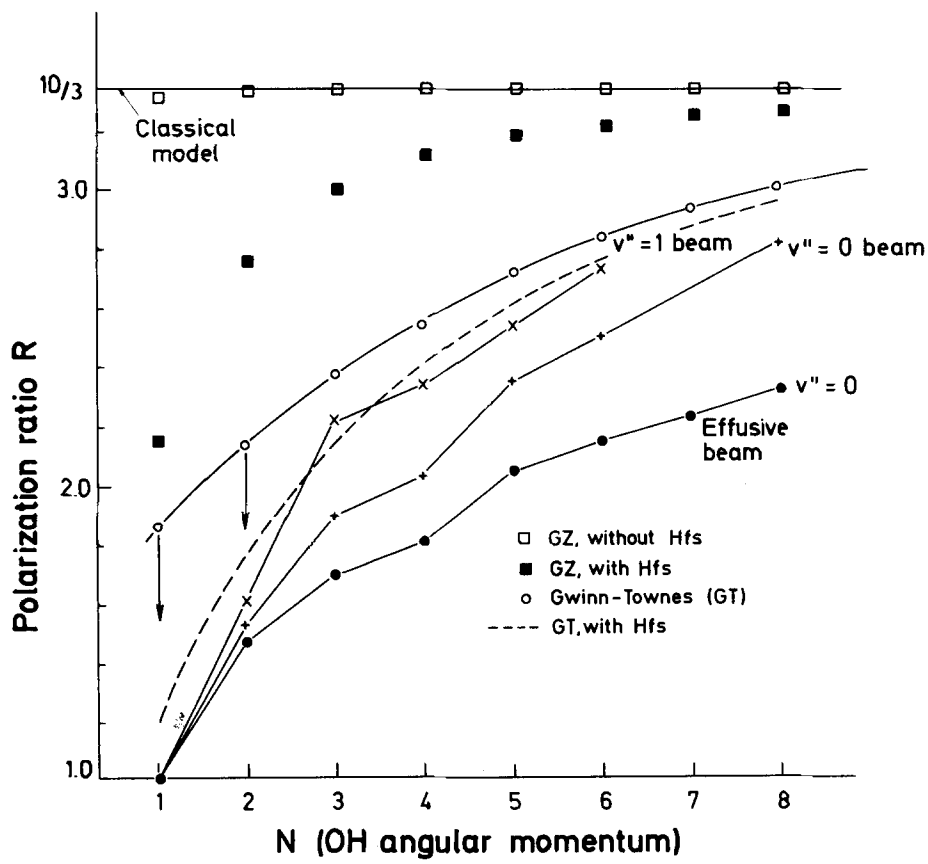

FIG. 13. Experimental and theoretical results for the polarization. Plotted are the ratios of fluorescence intensities, measured and predicted, with $\epsilon_E \| \epsilon_D$ and $\epsilon_E \perp \epsilon_D$ with the detector along the Y axis (our case a/case b). The lower three curves [$v'' = 0$ effusive beam (●), $v'' = 0$ beam (+), $v'' = 1$ beam (x)] represent experimental results. The horizontal line at 10/3 is the result of a classical calculation, the open squares near that curve represent the results of quantum calculations according to the formalism of Greene and Zare. Modifications of the prediction for (a) hyperfine structure, and (b) direction of the OH transition moment are discussed in the text. The broken line should be compared to the data, except for $N = 1,2$, where the arrows indicate, that because of satellite line overlap, the calculated values are too large.

and $E_v(n)$ is the vibrational energy of OH in a given quantum state n. As a reasonable approximation for E^P_{int} we choose $3/2\ kT$. Although this value is small relative to the photon energy, the details concerning which rotational states of H_2O are populated at a given temperature will be required to analyze the influence on the final rotational distribution of the OH fragments. Bond dissociation energies of 5.119 and 5.205 eV were used for H_2O and D_2O, respectively.[29]

The fraction of energy partitioned into OH vibration was the same regardless of the initial temperature of H_2O. From the measured distribution this fraction is $f_V = 0.095 \pm 0.005$. In other words nearly 10% of the available energy is partitioned into OH vibrational excitation.

Partitioning of energy into OH rotation depends very much on the initial H_2O temperature as well as the final state of OH produced. The fractions f_R for OH in different vibrational and Λ-doublet states from $H_2O(T_{\text{int}})$ are listed in Table IV. The values for the $^2\Pi_{1/2}$ spin state are not included because the same basic trend is observed as the $^2\Pi_{3/2}$ state. Table IV is basically another way of writing Table III which lists the effective temperatures of the OH radicals. Because of the non-Boltzmann behavior of the data, average rotational energies are more reliable parameters to represent the data, although less informative.

Because E_{aval} is too small to permit electronically excited $OH(A\ ^2\Sigma^+)$ formation, conservation of energy permits us to write the fraction of energy released as relative translation of the H and $OH(X)$ fragments as $f_T \sim 0.9$. Here we assume $f_R \sim 0.02$ realizing the finer details of Table IV will not alter this value much. So the major energy channel is relative translation of which 17/18 of E_T will be carried by the H atom. The translational energy distribution was not measured directly here, but the narrow rotational and vibrational distributions imply that the translation has only a $\pm 6\%$ energy spread.

Summarizing, we measure the energy partitioning for the photodissociation products to be

$$f_T : f_V : f_R = 0.885 : 0.095 : 0.02.$$

B. Internal state distributions

1. Vibrational distributions

We observe almost equal populations in $v'' = 0$ and $v'' = 1$ and a significant amount in $v'' = 2$. This large amount of vibrational excitation is rather surprising, but can be explained through a final state interaction on the excited potential surface.

Free OH is similar to that bound to an H atom in the ground state water molecule. The OH stretching frequencies ($\nu_1^s = 3\ 657\ \text{cm}^{-1}$, $\nu_3^a = 3\ 755\ \text{cm}^{-1}$) and equilibrium bond length ($r_e = 0.956$ Å) of water[30] are not much different from the vibrational frequency and bond length of the free radical[31] ($\nu = 3735\ \text{cm}^{-1}$, $r_e = 0.9706$ Å). Therefore, neither sudden[32] nor Franck–Condon[33] models predict appreciable vibrational excitation. If one of the OH bonds is suddenly cut, and the free OH retains its previous geometry in the H_2O, very little vibrational excitation can result.

The quasidiatomic impulsive model[34] also predicts essentially no vibrational excitation in the fragment OH radical. This is because the HOH angle is close to 90° so any force exerted on the oxygen atom by the departing H atom has only a small component along the remaining OH bond, and thus fails to compress or stretch the OH "spring."

The models mentioned above, which work reasonably well for asymmetric triatomic molecules such as HCN,[33] are found to fail for the symmetric H_2O case, which has two equivalent OH bonds. Considerations of the molecular orbitals involved in the water tell us that vibrational excitation may be expected. Our initial transition in water takes an electron from the nonbonding $1b_1$ to an antibonding $4a_1^*$ orbital (see Fig. 2 at the left), which has nodal planes between the oxygen and the two hydrogen atoms. As indicated by the arrows along the OH bonds both hydrogen atoms are repelled initially, resulting in the excitation of a symmetric stretch. For energetic reasons however, only one H atom can leave the excited complex, so that the vibrational energy remains in OH. This explains qualitatively the observed vibrational excitation.

TABLE IV. Energy disposal into product rotation.

Dissociation product[a]	H_2O temperature (K)	$E_{\text{aval}}(\text{cm}^{-1})$	$E_r(\text{cm}^{-1})$	$f_R(\%)$
$OH(^2\Pi_{3/2}, v'' = 0)$[b]	300	22 731	478.2	2.10
$OH(^2\Pi_{3/2}, v'' = 1)$[b]	300	19 161	456.7	2.39
$OD(^2\Pi_{3/2}, v'' = 0)$[b]	300	23 451	507.1	2.16
$OH(^2\Pi_{3/2}, v'' = 0)$	260[c]	22 671	359.9	1.59
$OH(^2\Pi_{3/2}, v'' = 0)$	260[c]	22 671	287.2	1.27
$OH(^2\Pi_{3/2}, v'' = 1)$	260[c]	19 102	301.96	1.58
$OH(^2\Pi_{3/2}, v'' = 1)$	260[c]	19 102	262.3	1.37
$OH(^2\Pi_{3/2}, v'' = 0)$	10	22 411	302.7	1.35
$OH(^2\Pi_{3/2}, v'' = 0)$	10	22 411	153.3	0.68
$OH(^2\Pi_{3/2}, v'' = 1)$	10	18 841	239.6	1.27
$OH(^2\Pi_{3/2}, v'' = 1)$	10	18 841	128.6	0.68

[a] Results for the $^2\pi_{1/2}$ spin state were not significantly different and are not included in this already lengthy table.

[b] Both Λ doublets were equally populated at room temperature.

[c] This temperature is an estimate and not well defined.

Another way to discuss the same situation is to consider the excited $^1B_1$ potential energy surface. Because of the H_2O symmetry, the saddle point of the excited surface lies along the bisector, which is the symmetric stretching coordinate. Since electron density is placed in an antibonding orbital, the bond order is reduced and the OH bond will be longer in the $^1B_1$ state than in the $^1A_1$ state, i.e., the saddle point will be further out along the symmetric stretching coordinate of the $^1B_1$ state than the well of $^1A_1$ state. Preliminary results of *ab initio* calculations[45] by Stämmler (private communication) do show this behavior. Therefore, a Franck–Condon excitation places the molecule on a steep repulsive wall, and it initially follows the symmetric stretch coordinate. Only after the molecule finds its way into the asymmetric stretch coordinate (reaction coordinate) can it dissociate. This "vibrational predissociation" model[35] appears to be a general feature of symmetric (and nearly symmetric) triatomic molecules and indeed many ABA molecules studied, have vibrationally excited AB photofragments (H_2S,[36] NO_2,[37] O_3,[38] CO_2,[39] HgX_2,[40] SO_2,[41]). The degree of vibrational excitation is very sensitive to the position of the saddle point relative to the ground state well and to the slope of the repulsive wall of the $^1B_1$ state.

2. Rotational distribution

The rotational distributions of the product OH shown in Fig. 11 depend strongly upon the initial rotational temperature of the H_2O.

There is almost no rotation in the internally cold H_2O which constitute the nozzle beam, so that the rotational excitation of OH is exclusively due to the dissociation on the $^1B_1$ potential energy surface. In this case we prepare a well defined initial state of H_2O^* and analyze the final state of OH after the dissociation. This corresponds to state-to-state cross sections in scattering and thus these rotational distributions should give the most sensitive check for a comparison with theory.

Both for the effusive beam and the cell there is a distribution of rotational states in H_2O prior to dissociation. As may be seen from Table III the rotation of the parent goes to the product OH: The rotational temperature of OH increases from 475 to 930 K going from the nozzle beam to the cell (Q lines). The rotational temperature increase in H_2O is smaller than 300 K, whereas it is 450 K in OH. It is obviously not *only* the parent rotation that is transferred to the product. It may be that with increasing rotational energy of the parent another part of the potential energy surface is sampled by the trajectories leading to more rotational excitation in the product.

On the whole there is very little rotational excitation of OH. The impulsive model,[34] which failed to describe the relatively large degree of vibrational excitation, seems to do a better job here because it predicts only a small fraction of rotational energy. This is because the c.m. of the OH is very near the oxygen atom, so any force exerted on the oxygen will only produce a small torque. However, the predicted fraction of rotational energy f_R is an order of magnitude too low and grossly underestimates the population of the higher rotational states. Stronger evidence against this model is that it predicts a factor of 4 more rotational energy in OD in the dissociation of D_2O, while we find essentially no difference (see Fig. 9).

A simple Franck–Condon model which included bending contributions was applied by Beswick and Gelbart[42] to the dissociation dynamics of H_2O. Although their general trend of decreasing OH angular momentum with decreasing H_2O rotation was observed here (see Fig. 11) their predicted oscillations were not seen. As in the case of H_2S,[43] this lack of oscillations is due to the neglect of the final state interactions, which play the dominant role here. That final state interactions are important can also be seen from the photodissociation of H_2O in the second absorption band,[6,7] where much more OH rotational excitation is observed in the product OH. Although the kinematics are identical here, the dissociation occurs from another potential energy surface, that is responsible for the differences.

In the previous discussion of the excited state surface, the two stretching coordinates were considered, and their inseparability shown to produce vibrational excitation. There is also a third coordinate to be considered, corresponding to the HOH bending vibration, which is reponsible for the OH rotational excitation.

According to Walsh's rules,[44] H_2O is bent in the ground state but, upon excitation of an electron to the next orbital, will be more stable with a linear configuration. This "need to become linear" is an excitation of the bending vibration of excited H_2O and such a motion will cause the OH to rotate more than expected from a force directed along the bonds. *Ab initio* calculations[45] on the $^1B_1$ state support the Walsh's rule conclusion that the linear configuration of water is energetically favored, although only if both OH distances are larger.

Consider also the relevant time scales. Even for the highest rotational state of OH the rotational period is ~ 0.2 ps which is much slower than the departure time of the H atom (~ 0.02 ps). Thus the OH can not rotate more than $\sim 30°$ and the trajectories will sample only HOH angles in the range of $105° \pm 30°$. During the whole dissociation process we will not reach the collinear HOH configuration, where a conical intersection with the $^1A_1$ state occurs.

The rotational distributions are very similar for both vibrational states of the OH fragment. This observation reflects the fact that the vibrational excitation is mainly due to the symmetric and antisymmetric stretch coordinates, whereas the bending coordinate is responsible for rotational excitation independent of the stretching motions.

A closer look at the 300 K data (Figs. 8 and 10) shows that there is a slight curvature at low rotational states, that is more pronounced in the case of D_2O. This curvature at low N'' is not found in Fig. 11 for cold water. This behavior can be explained by assuming that the initial parent rotation will mainly be transferred to the lower rotational states of the OH product.

However there is a complication that arises from the overlap[17] of main branch and satellite lines which occurs in the low rotational states. We work in saturation with a three-level system and obtain equal populations in each level. Thus the excitation probability will be 2/3 instead of 1/2 so that

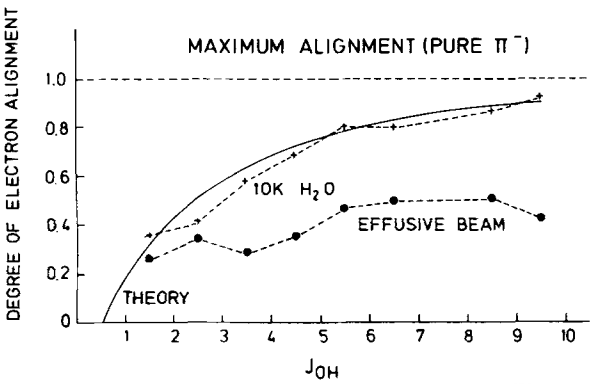

FIG. 14. Degree of electron alignment as a function of J_{OH}. Water at 10 K is represented by +, warmer H_2O by ●. The experimental values are the ratios of fluorescence intensities $(Q - R)/(Q + R)$ at each J_{OH}, while the data are those of Fig. 12. The solid line is calculated from the Gwinn–Townes coefficients via $2c_J^2 - 1$. No allowance has been made for the presence of satellite lines at $J_{OH} \leqslant 2.5$.

the apparent higher population at low rotational states may not be true in the 300 K case. The pronounced curvature in the R branch for the cold water will be discussed in relation to the Λ-doublet population. Nevertheless, the difference between the 300 and 10 K data at low N'', cannot be explained by this overlap.

Finally we want to discuss why a single parameter, such as the rotational temperature can describe the measured distributions. *A priori*, there is no reason to expect a statistical distribution from such a direct and selective process. Nevertheless this behavior has often been found (e.g., OH from H_2O_2 at 248 nm,[46] SH from H_2S at 193 nm,[43] and OH from HONO at 369 nm[47]). Even in the ground state of the parent molecule there is still zero-point motion, giving an initial statistical distribution for starting trajectories. Depending on these initial conditions the trajectories sample different parts of the potential surface and are distributed over different rotational states. Unless there is a mechanism that selectively populates definite rotational states there is no reason to expect deviations from statistical behavior. Statistical behavior is more likely with higher parent temperatures, since the range of starting trajectories is larger. However, this depends on the details of the potential surface, and indeed, in other cases non-Boltzmann behavior is found (NO from NO_2 at 337 nm,[37] CN and NO from NOCN at 532 nm,[48] and OH from H_2O_2 at 193 nm[46]).

3. Spin distribution

Although the spin distributions in Fig. 9 look more or less statistical, there might be a slight preference for the $^2\Pi_{1/2}$ state at low N'' for $v'' = 0$ and at all N'' for $v'' = 1$. Although in the isoelectronic molecule H_2S a strong preference for the $^2\Pi_{3/2}$ state is found[43] our effects are comparatively small. A spin preference has also been observed in several other photodissociation processes (HONO,[47] NOCN,[48] and NO_2[37]).

4. Distribution among the Λ doublets

In Sec. II we gave a brief explanation for the dramatic preferential population of the upper Π^--Λ doublet (see Fig. 3) in terms of the symmetry conservation of the electronic wave function during the dissociation: the $1b_1$ electron of the excited H_2O goes to the unpaired $p\pi$ lobe of OH that is perpendicular to the OH rotation plane. This explanation however holds only at large OH angular momenta (we observe an increasing fraction of molecules in the Π^+ state as J_{OH} is reduced) and only for the case of internally cold H_2O. Due to the important implications for both the dissociation dynamics and the astronomical OH maser we will discuss in this section: (a) the origin of the Λ-doublet splitting and the Λ-doublet mixing, (b) the controversy about the orientation of the unpaired $p\pi$ lobe of OH for the two Λ-doublet states; (c) the strong J dependence of the Λ-doublet population for the cold H_2O, and (d) the effect of initial rotation of H_2O upon the Λ-doublet distribution.

a. Λ doubling and Λ-doublet mixing in OH. The ground electronic wave function $^2\Pi$, $[...(2s\sigma)^2(2p\sigma)^2(2p\pi)^3]$ of OH can be either symmetric or antisymmetric relative to a reflection at a plane through both nuclei. This gives rise to two degenerate quantum states—the two Λ-doublet states—if no rotation occurs. However, if the molecule rotates, a coupling of the electronic motion with the nuclear rotation causes a splitting of the Λ-doublet states. Clearly the Λ-doublet splitting cannot be described in terms of the Born Oppenheimer approximation which neglects any such interactions.

In the high-J limit we can identify the two Λ-doublet states with the oriented singly occupied $p\pi$ lobes shown at the right of Fig. 2. The $p\pi$ lobe perpendicular to the OH rotation plane gives the antisymmetric Π^- state, whereas the $p\pi$ lobe in plane gives the symmetric Π^+ state. We define a degree of electron alignment in Fig. 14 which is unity for the pure Π^- state. The symmetry element here is the OH rotation plane. For the Π^+ state the unpaired $p\pi$ lobe is rotating with the OH molecule giving a donut shape for the electronic orbital. For the Π^- state however the $p\pi$ lobe has a node in the plane and does not change its shape with the OH rotation. This implies that for the description of the Π^+ state mixing with a nearby Σ state has to be introduced, whereas the Π^- state remains unchanged.[10]

At lower J however, this simple picture breaks down. Instead, both the Π^- and Π^+-Λ-doublet states are mixtures of these two limiting cases ("Λ-doublet mixing"). We describe the unpaired $p\pi$ lobe perpendicular to the plane as proportional to $\cos\phi$ and that in the plane as proportional to $\sin\phi$, where ϕ is the angle in the X,Y plane which is perpendicular to the molecular axis Z, measured from the Y axis (compare Fig. 15). We then write the wave function at intermediate J,

$$\psi = c_J \cos\phi + d_J \sin\phi, \tag{12}$$

where c_J and d_J are J-dependent mixing coefficients. We are concerned only with the ϕ dependence of ψ here.

The high-J limit with the oriented unpaired $p\pi$ lobes is obtained by

$$\begin{aligned} &c_J = 1, \quad d_J = 0: \quad \psi = \cos\phi \quad (\perp\text{OH–POR}) \\ &c_J = 0, \quad d_J = 1: \quad \psi = \sin\phi \quad (\parallel\text{OH–POR}), \end{aligned} \tag{13}$$

c_J^2 and d_J^2 represent the probability of finding the unpaired $p\pi$ lobe perpendicular to, or in the plane, respectively. This Λ-doublet mixing was discussed by Gwinn *et al.*[49] to determine the degree of alignment in the X,Y plane of the un-

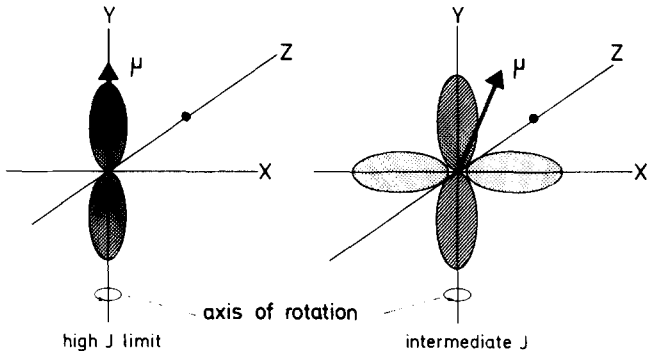

FIG. 15. Direction of the transition moment in OH for Q lines. In the high-J limit (left side) the transition moment μ is along the $p\pi$ lobe. At lower J the transition moment has an angle in the (X, Y) plane due to mixing of the Λ-doublet states.

paired $p\pi$ lobe for intermediate J.

To quantify this degree of alignment the authors used the quantity

$$\Delta = \langle\psi| Y^2 - X^2 |\psi\rangle, \tag{14}$$

which is related to the difference of electron densities along Y and along X (compare Fig. 15 for the coordinate system). For $\psi = \cos\phi$ we obtain $\Delta = +0.5$, for $\psi = \sin\phi$ we obtain $\Delta = -0.5$ and for $c_J = d_J$ we obtain $\Delta = 0$. Thus Δ is a convenient measure for the alignment of the π lobe: if $\Delta = -0.5$ the π lobe is aligned along X, if $\Delta = 0$ we have no alignment and for $\Delta = +0.5$ the π lobe is aligned along Y. The values of Δ are given for OH in Table I of Ref. 49. From these values we can obtain the expansion coefficients by

$$c_J^2 = 0.5 + \Delta \quad \text{and} \quad d_J^2 = 0.5 - \Delta. \tag{15}$$

In this way the wave function ψ is completely determined.

The same quantity Δ has been used by Townes *et al.*[50] who treated the alignment of the unpaired $p\pi$ lobe for a molecule that undergoes a transition from Hund's case (a) at low J_{OH} to Hund's case (b) at large J_{OH}. They expanded the wave functions in terms of Hund's case (a) wave function $\Pi_{1/2}$ and $\Pi_{3/2}$:

$$\psi = a_J \Pi_{1/2} + b_J \Pi_{3/2}, \tag{16}$$

and obtained almost exactly the same numerical result for Δ as Gwinn *et al.*[49] For the product of the mixing coefficients a_J and b_J they found that

$$a_J \cdot b_J = \left[4 + \frac{(\lambda - 2)^2}{(J - \frac{1}{2})(J + \frac{3}{2})}\right]^{-1/2} = \Delta \tag{17}$$

with $\lambda = A/B$. A is the spin-orbit splitting coefficient and B the rotational constant of the molecule. Equation (17) describes a transition from Hund's case (a) to Hund's case (b): If $J \to \infty$ we find $a_J b_J \to 0.5$ which means (because $a_J^2 + b_J^2 = 1$) that $a_J^2 = b_J^2 = 0.5$. Thus in the high-J limit the distinction between the two Hund's case (a) wave functions is gone. For $J = 1/2$ however, we obtain $a_J b_J = 0$ which corresponds to $a_J = 1$ and $b_J = 0$. Only in this case is there a true Hund's case (a) wave function $\Pi_{1/2}$.

The coefficients a_J, b_J are related to the c_J, d_J by

$$c_J^2 = 0.5 + a_J b_J = 0.5 + \left[4 + \frac{(\lambda - 2)^2}{(J - \frac{1}{2})(J + \frac{3}{2})}\right]^{-1/2}. \tag{18}$$

From this equation, it is clear that $c_J^2 \to 1$ as $J \to \infty$. The rate of convergence depends very much upon the size of λ. The approach to the high-J limit is different for each molecule: it is fast for CH($\lambda = +3.58$), moderate for OH($\lambda = -7.36$), slow for SH($\lambda = -39.9$), and very slow for NO($\lambda = +73.6$).

It is interesting to note, that the orientation of the unpaired $p\pi$ lobe increases with J and that the J dependence parallels that of the transition of the molecule from Hund's case (a) to Hund's case (b). The implications of this result upon Λ-doublet population and polarization will be discussed below.

b. Orientation of the unpaired $p\pi$ lobe in the two Λ-doublet states. There has been considerable confusion in the literature concerning the relation between the energetic ordering of the Λ doublets and the orientation of the unpaired $p\pi$ lobe in the free OH. In the first theoretical attempt[49] to obtain a relation between the orientation of the unpaired $p\pi$ lobe and the energetics of the two Λ doublets, Gwinn *et al.* predicted that the upper Λ-doublet level belongs to a configuration where the unpaired $p\pi$ lobe is located in the OH-rotation plane.

Although for a $p\pi^1$ electronic configuration there is general agreement that the upper Λ doublet correlates to the unpaired $p\pi$ lobe perpendicular to the OH rotation plane, these authors,[49] and others,[50–53] claim that for a $p\pi^3$ configuration the energetic ordering is reversed. As discussed above, they also showed that only in the high-J limit is there a well defined orientation of the unpaired $p\pi$ lobe relative to the OH rotation plane, and that at intermediate J_{OH} there is a strong mixing of the Λ doublets.

First experimental evidence for an orientation effect of the unpaired $p\pi$ lobe of OH was found by Luntz *et al.* in the chemical reaction $H + NO_2$.[54] They probed the OH by LIF and found more intensity on P and R lines than on Q lines. From the well established spectroscopy of OH,[16,17] there is no doubt that P and R lines measure the population in the *lower* Λ-doublet level, whereas Q lines measure the population in the *upper* Λ-doublet level. Because the reaction $H + NO_2$ proceeds via a planar HONO intermediate it is reasonable to assume that the ON-bond breaks in the plane, leaving the unpaired $p\pi$ lobe preferentially aligned in the OH-rotation plane (the OH and HONO planes are parallel). This supports its identification with the P and R lines and consequently with the lower Λ doublet. The reaction $H + NO_2$ has also been treated by Kinsey *et al.* Despite the strong evidence for this orientation effect, Kinsey *et al.* confused the correct assignment of the Λ doublets. An even better example for this orientation effect is the reaction of $O^1D + H_2$[54] which necessarily has to be planar and produces a strong preference for the lower Λ doublet. Other chemical reactions producing OH($^2\Pi$) were almost always found to preferentially populate the lower Λ doublet. So, for example, the reaction of $H + H_2O$, that was originally suggested to explain the pump mechanism of the astronomical OH maser, was recently shown by Kleinermanns *et al.*[58] to give a preferential population of the lower Λ-doublet level.

Our data are the *first* experimental observation of a preferential population of the upper Λ-doublet level (prefer-

ence for Q lines). One explanation for this inversion is based upon an argument (presented in Sec. II) about the orientation of the unpaired $p\pi$ lobe similar to that used for chemical reactions: at 157 nm we create an unpaired $p\pi$ lobe *perpendicular* to the H_2O plane which should remain perpendicular to the plane of the free OH. On the other hand, we find more population in the upper Λ-doublet state, which is measured by the Q line intensity, suggesting that for the upper Λ doublet the unpaired $p\pi$ lobe is perpendicular to the rotation plane. This picture supports the mechanism proposed for chemical reactions[53,54] and contradicts the earlier theoretical work.[49,50]

These qualitative arguments are pictorial and attractive. However a more direct confirmation is that we *measure* the orientation of the unpaired $p\pi$ lobe relative to the OH-rotation plane in our polarization experiment. These experiments were done with Q lines. For high J_{OH} we obtain ~ 3 times more LIF intensity at the PMT if the electric vector ϵ_E of the OH probe laser is perpendicular to the OH rotation plane (compare Fig. 4).

This demonstrates that for the upper Λ-doublet state, which is measured via Q lines, the transition moment is perpendicular to the OH rotation plane. It remains to be shown that the transition moment is along the unpaired $p\pi$ lobe, because *then the unpaired $p\pi$ lobe is perpendicular to the OH rotation plane for the upper Λ doublet.*

This is shown by introducing the operator $\tilde{P}$ for the reflection of the electronic wave function at the OH rotation plane. For $\psi = \cos\phi$ (unpaired $p\pi$ lobe perpendicular to the OH-rotation plane) we obtain for the transition moment

$$\left\langle \cos\phi \left| \begin{matrix} m_x \\ m_y \\ m_z \end{matrix} \right| \Sigma \right\rangle = \left\langle \tilde{P}\cos\phi \left| \begin{matrix} \tilde{P}m_x \\ \tilde{P}m_y \\ \tilde{P}m_z \end{matrix} \right| \tilde{P}\Sigma \right\rangle$$

$$= \left\langle -\cos\phi \left| \begin{matrix} +m_x \\ -m_y \\ +m_z \end{matrix} \right| \Sigma \right\rangle = \begin{matrix} - \\ + \\ - \end{matrix} \left\langle \cos\phi \left| \begin{matrix} m_x \\ m_y \\ m_z \end{matrix} \right| \Sigma \right\rangle .$$

Only for the Y direction is this transition moment nonzero and thus perpendicular to the plane. In the same way it can be shown that for $\psi = \sin\phi$ (unpaired $p\pi$ lobe in the OH rotation plane) the transition moment lies in the OH rotation plane. This proves conclusively that for the upper Λ doublet in the high-J limit the unpaired $p\pi$ lobe is perpendicular to the OH-rotation plane.

c. J dependence of the Λ-doublet population. In this section we will discuss the strong J dependence of the Λ-doublet populations for internally cold H_2O. The decrease of the population inversion with increasing H_2O temperatures will be treated in the next section.

As mentioned in Sec. II, the Π^- state of the free OH correlates to the excited $^1B_1$ state of H_2O, whereas the Π^+ state correlates to the ground-state $^1A_1$. The correlation is due to the symmetry relative to a reflection of the electronic wave function at the OH rotation plane (which is identical to the H_2O plane for internally cold H_2O). The strong preference for the population of the Π^- state was explained qualitatively by the conservation of this symmetry during the dissociation.

Obviously this symmetry selection rule holds rigorously only in the high-J limit where we observe almost exclusively the Π^- state. However, at lower J, appreciable population in the Π^+ state also occurs indicating that symmetry is not conserved. The explanation for this J dependence is related to the Λ-doublet mixing in the free OH molecule discussed in the preceding section, and to the degree of similarity of the $1b_1$ electron in H_2O with the wave functions of Eq. (12) for the free OH. We assume here that the overlap integral

$$\langle 1b_1|\psi\rangle \tag{19}$$

of the $1b_1$ electron in the excited $^1B_1$ state of H_2O and the eigenfunctions of Eq. (12) of the free OH represents the probability for a transition from the initial state $|1b_1\rangle$ to the final state $|\psi\rangle$ of OH. This may be justified in the following way.

In the Born–Oppenheimer approximation to the Schrödinger equation the coupling term $\langle\varphi_i|\tilde{T}_K|\varphi_f\rangle$, which describes the interaction of the electrons with the nuclei, is neglected. φ_n are solutions of the electronic Schrödinger equation, assuming that the nuclei are at rest and $\tilde{T}_K$ is the operator for the kinetic energy of the nuclei. If we assume that the out-of-plane orbital ($1b_1$ in H_2O) does not change much with the internuclear distances, it can be shown that the coupling is proportional to the overlap integral in Eq. (19). As a first approximation it is reasonable to assume that the probability for a transition from $|\varphi_i\rangle$ to $|\varphi_f\rangle$ is given by this coupling.

If we consider the high-J limit [Eq. (13)] with the two oriented unpaired $p\pi$ lobes $\psi = \cos\phi$ and $\psi = \sin\phi$ we obtain immediately

$$\langle 1b_1|\cos\phi\rangle = 1 \qquad (\Pi^-)$$
$$\langle 1b_1|\sin\phi\rangle = 0 \qquad (\Pi^+),$$

because the $1b_1$ electron is quite well described by $\cos\phi$. Thus in the high-J limit we find only population in the Π^- state.

For intermediate J however, we can no longer use the limiting eigenfunctions but instead need the linear combinations from Eq. (12). Then we obtain for the Π^- state

$$\langle 1b_1|\psi\rangle = \langle\cos\phi\,|c_J\cos\phi + d_J\sin\phi\rangle = c_J,$$

and c_J^2 represents the probability for a transition to the Π^- state. Correspondingly $d_J^2 = 1 - c_J^2$ represents the probability to obtain the Π^+ state.

The ratio for the population in the Π^- relative to the Π^+ state will thus be given by

$$\frac{\Pi^-}{\Pi^+} = \frac{c_J^2}{1 - c_J^2}, \tag{20}$$

where the c_J^2 are obtained from Eq. (18) using the known spin-orbit and rotational constants of OH (there are no free parameters).

The theoretical curve obtained from Eq. (20) is also plotted in Fig. 12 and shows excellent agreement with the experimental result. The strong J dependence of the Λ-doublet inversion is thus explained by the orientation of the unpaired $p\pi$ lobe in OH which is determined by the coefficients c_J^2. The data are also plotted as "degree of electron alignment" in Fig. 14.

This result has important implications:

(1) The simple model presented here holds for cold H_2O, where we have a completely planar dissociation. The nice agreement between experiment and theory is not expected if out-of-plane rotations are present. This demonstrates that the use of nozzle beams can be very important in photodissociation studies.

(2) For similar studies with other molecules, such as H_2S in the first absorption band, the theory would predict a very different J dependence. Because λ is larger for SH, its transition from Hund's case (a) to Hund's case (b) is much slower, and the model predicts a much less pronounced Λ-doublet inversion. For example, Houston's experiment with a cold beam[43] produced $J = 4.5$ as the highest rotational state observed with reasonable intensity and found no population inversion. Our model predicts a ratio of $\Pi^-/\Pi^+ = 1.6$ which may be difficult to measure. However, it is also possible that another potential surface is involved.

(3) A very useful tool for the analysis of chemical dynamics may result from the application of our model. For most of those reaction products found to have nonstatistical Λ-doublet populations, a larger effect is found with increasing J. As mentioned above, the qualitative explanation for any preference is a planar reaction intermediate in which a bond breaks in plane, leaving an unpaired $p\pi$ lobe oriented *in plane*. To explain the J dependence in this case, we have to use the unpaired $p\pi$ lobe in plane, rather than the out-of-plane $1b_1$ electron of H_2O used in the overlap integral of Eq. (19). We believe that this explains qualitatively the J dependence of the Λ-doublet population in chemical reactions: it is not due to nuclear dynamics; it is due to Λ-doublet mixing in the product molecule.

In chemical reactions, however, the processes are not as simple as the dissociation considered here, in which a cold H_2O must be completely planar. The impact parameters lead to a range of orbital angular momenta, so that the "collision plane" (defined, e.g., by the three particles of $O + H_2$) can rotate during the collision, corresponding to an out-of-plane rotation in the photodissociation. As discussed below, the out-of-plane rotations in the photodissociation smear out the preference for one Λ-doublet state. Thus, for chemical reactions we expect that the maximum preference for one Λ doublet is determined by the planarity of the process. Due to the contribution of more angular momenta, the preference for one Λ doublet should be less than in our case of cold H_2O.

As previously discussed, the approach of a molecule from Hund's case (a) to case (b) with J can be slow or fast depending upon the parameter λ of the molecule. For example NO approaches Hund's case (b) very slowly and thus will have only a very weak preferential Λ-doublet population at lower J. Accordingly, we expect the J dependence in the Λ-doublet population for chemical reactions to approach the high-J limit at the same rate that the molecule shifts from Hund's case (a) to Hund's case (b).

We believe this model can be used to study the planarity of chemical reactions and provide information about the range of impact parameters that contribute to the reaction.

d. Influence of initial H_2O rotations on the Λ-doublet population. At a first sight it is surprising that the Λ-doublet population, which is an electronic property, depends upon the rotation of the nuclei. If the Born–Oppenheimer approximation would hold the electrons would adjust immediately to the positions of the nuclei, independent of nuclear rotation.

However, the entire effect of Λ doubling can not be explained in terms of the BO approximation because it does not consider the coupling of the electrons to the motion of the nuclei, i.e., motion of the nuclei is neglected in the BO approximation. Thus it is *not necessary* to obtain the same Λ-doublet population for different initial rotations of H_2O.

Nevertheless it is startling that the rotational energy existing in H_2O at 300 K is enough to completely destroy the population inversion (see Fig. 12). To understand this, a consideration of the relevant time scales is important.

The rotational period of the H_2O molecule is very short because of the small moment of inertia. However, the photon absorption can be considered immediate and photoselects an H_2O plane in space, with the $1b_1$ orbital perpendicular to this plane. The rotation of the H_2O plane will continue after the photon absorption, but will slow down and finally stop because the moment of inertia (around the CM of H_2O) increases as the H_2O falls apart. After the separation is complete, there will be an angle γ between the photoselected initial plane and the final plane.

An estimate for γ can be obtained in the following way. The average rotational period τ_r of the H_2O is ~ 0.2 ps, whereas the time for the separation τ_s of the H atom is ~ 0.02 ps. Thus a rough estimate for the lower limit for γ is

$$\gamma \leqslant \frac{\tau_s}{\tau_r} \cdot 360^\circ \sim 30^\circ. \tag{21}$$

The OH will rotate in the final plane, and the eigenfunction ψ from Eq. (12) will be oriented at this final plane, whereas the $1b_1$ electron will be oriented at the initial plane.

As before we assume that a transition from the initial state $|\varphi_i\rangle = |1b_1\rangle$ to the final state $|\varphi_f\rangle = |\psi\rangle$ has the probability $\langle 1b_1|\psi\rangle$. However, because of the angle γ between the photoselected initial and the final planes, the overlap will be very different because the unpaired $p\pi$ lobes in H_2O and OH will now have an angle γ relative to each other. In this way, even for moderate angles the population inversion can be smeared out to a considerable extent.

The sensitive dependence of the Λ-doublet population upon the H_2O rotations demonstrates that in the case of the cold H_2O initial out-of-plane rotations are obviously not important.

In the effusive beam the Λ-doublet inversion is much less because out-of-plane rotations become important and so γ is finite. In the cell the out-of-plane rotations are even more important and completely destroy the Λ-doublet inversion.

The Λ-doublet population inversion is very sensitive to out of plane rotations and it might be possible to determine an average angle γ between the initial and the final plane of H–OH.

An important aspect of the temperature dependence of the Λ-doublet population is that the pump mechanism for the astronomical OH maser is most efficient at lower rotational temperatures of H_2O, which exist in space.

C. Polarization discussion

The experimental results for the polarization ratio R are described in Sec. IV and are displayed in Fig. 13. Also shown are five different theoretical curves, which were calculated on the basis of completely planar dissociation dynamics ($\beta = 2$ in our classical model).

The horizontal line at the top is that predicted from the classical model outlined previously for $\beta = 2$, i.e., for the $\cos^2\theta$ distribution of J_{OH} pictured in Fig. 2. The open squares are the result of the Greene–Zare quantum calculations[24] for the same situation. The closed squares include corrections to the GZ treatment for the effect of proton hyperfine structure (hfs) upon the absorption and emission process, according to their Eqs. (23) and (24).[59] This depolarization effect arises because J_{OH} now precesses around F.

The experimental data all show an increasing deviation from these theoretical predictions with decreasing N''. The $+$ and x indicate data for $v'' = 0$ and 1, respectively, obtained from the 10 K beam. It might be thought that the deviations at low N'' are due to quantum effects, but the GZ calculations indicate that their influence is negligible here. The effect of the hyperfine structure is greater, but still insufficient to explain the data.

The reason for these deviations in the J dependence is related to the Λ-doublet mixing in OH that was discussed in Sec. V. Using the wave functions of Eq. (12) to determine the transition moment μ_E we obtain

$$\mu_E = \langle \psi | \tilde{m} | \Sigma \rangle = \langle c_J \cos\phi + d_J \sin\phi \, | \tilde{m} | \Sigma \rangle$$
$$= c_J \langle \cos\phi \, | \tilde{m} | \Sigma \rangle + d_J \langle \sin\phi \, | \tilde{m} | \Sigma \rangle. \quad (22)$$

As mentioned before the matrix element $\langle \cos\phi \, | \tilde{m} | \Sigma \rangle$ is perpendicular to the OH rotation plane, whereas the matrix element $\langle \sin\phi \, | \tilde{m} | \Sigma \rangle$ lies in the OH rotation plane. At intermediate J's neither c_J nor d_J are zero, so that in general the transition moment is neither parallel nor perpendicular to the OH rotation plane. The angle μ_E makes relative to the OH rotation plane depends on the coefficients c_J from Eq. 18 and approaches the limiting cases that μ_E is parallel or perpendicular to the plane only at high J. As for the Λ-doublet population, the J dependence is typical for a given molecule and approaches the high-J limit at the same rate that the molecules goes from Hund's case (a) to case (b).

To include this effect in the classical model we treat the two components of the absorption dipole separately: One dipole perpendicular to the plane with the weight c_J^2, corresponding to the classical Q line excitation, and one dipole in the plane with the weight d_J^2 corresponding to a classical $P(R)$-line excitation. For the polarization ratio R we obtain in this case

$$R = \frac{c_J^2(7 + 41\beta/14) + d_J^2(6.5 - 17\beta/14)}{c_J^2(6 - 15\beta/7) + d_J^2(7 + 11\beta/7)}. \quad (23)$$

The terms with d_J^2, corresponding to $P(R)$-line excitation, can be derived either from the classical model described previously or from the high-J limit of GZ.

The result of this modification to the classical theory is shown in Fig. 13 as GT curve. It shows a strong J dependence that is exclusively due to Λ-doublet mixing. The same effect should occur in polarization experiments with other Π molecules and give rise to a J dependence of the polarization. The rate of approach of the polarization ratio to the high-J limit depends how quickly the molecule goes from Hund's case (a) to Hund's case (b).

However, to obtain the correct J dependence of R the hyperfine structure of OH also has to be considered. Multiplying the preceding GT curve by hfs depolarization factors (the values of *GZ, with hfs* divided by 10/3) gives the dashed curve called *GT, with hfs*. The agreement, especially with the $v'' = 1$ data for the dissociation from internally cold H_2O, is very good. This demonstrates that the strong J dependence in the polarization results is not due to any dynamic effects of the nuclei: we assume a completely planar dissociation process and obtain a strong J dependence. Although it is not as dramatic as in the Λ-doublet case, we see once again the importance of having the cold H_2O for comparison with theory.

The deviations of the theoretical curve in Fig. 13 at $N = 1, 2$ are readily explained: for the $Q_1 1$ and $Q_1 2$ lines we excite also satellite lines which show an opposite polarization behavior [like $R(P)$ lines] and cause a depolarization. This effect can not be treated quantitatively, because the *degree* of line overlap is difficult to determine. However, a rough estimate of this effect much improved the agreement for these points.

These measurements also show that: (a) the transition moment μ of H_2O in the first absorption band is perpendicular to the H_2O plane and (b) for Q lines in the high-J limit the absorption dipole is perpendicular to the OH rotation plane. This is especially important because it resolves the controversy about the orientation of the unpaired $p\pi$ lobe of OH in the two Λ-doublet states.

Some crude calculations were carried out to see if we can match the depolarization in the effusive beam case. These involve the out-of-plane rotations of the parent. The results of these calculations were in reasonable agreement with the depolarization, although it is rather easy to account for any depolarization because there are many potential causes. Nevertheless, the high degree of polarization remaining with the effusive beam indicates that the dissociation is very fast and takes place within $\sim 1/10$ of an out-of plane rotational period.

We would like to emphasize that our data analysis of the Λ doublets and the polarization involves *no adjustable parameters*: they are completely determined by the coefficients c_J^2 and d_J^2 which are characteristic for the free OH.

D. Application of Λ-doublet inversion to astronomical OH masers

The large population inversion of the Λ doublets found here from photolysis of cold water suggests the intriguing possibility that it may be responsible for OH maser action (near 18 cm) in the galactic environment.[60] Maser action occurs from the hyperfine levels of the ground rotational state of OH. As discussed in our preliminary report,[8] and by others,[49,50,60,61] once a population inversion is formed in the various rotational states, infrared relaxation to the ground rotational state maintains the inversion because of the $+ \leftrightarrow -$ selection rule. The low particle densities in space favor the

radiative relaxation. At higher densities collisional relaxation destroys the inversion,[62] as was observed in our experiments at high densities and/or long delay times.

Many theoretical attempts to explain the pump mechanism for the astronomical OH maser were incorrect because they used a wrong identification of the Λ doublets. This may be seen most clearly for the reaction $H + H_2O \rightarrow OH + H_2$ that was originally proposed by Gwinn *et al.*[49] to explain the Λ-doublet inversion in OH. Their basic idea was that this reaction should proceed via a planar intermediate with a chemical bond breaking in that plane, leaving OH with an unpaired $p\pi$ lobe in the OH rotation plane. In this paper we show that this corresponds to the lower Λ doublet *and not, as assumed, to the upper Λ doublet*. It was recently shown[58] that the reaction $H + H_2O$ does indeed give anti-inversion, consistent with the picture of an unpaired $p\pi$ lobe in the OH rotation plane. Much of the subsequent theoretical work was mislead by the erroneous assignment.

Nevertheless the pump mechanism proposed by Gwinn *et al.* has a number of advantages *because H_2O was involved*. The most important difference in our mechanism is that we use photons instead of fast H atoms to dissociate H_2O. Thus we keep the main advantages that are discussed in detail by Gwinn *et al.* and which are thus not repeated here.

The photodissociation mechanism requires VUV radiation and H_2O molecules, both of which are available, e.g., near new-born stars and OH masers have indeed been found in these regions.[63] Because the first absorption band has no detailed structure, a large spectral range of VUV radiation contributes to the inversion, in contrast to schemes presented by others[60] which require very narrow frequency ranges in the IR or UV.

A criticism of the dissociation mechanism[64] is its failure to include a scheme for the regeneration of the H_2O. One possibility may be $H_2 + OH \rightarrow H_2O + H$, whose rate constant is enhanced by vibrational[65] excitation and high kinetic energies, both of which are available here. Maser action is also found near comet tails[60] where H_2O is generated by evaporation of ice crystals.

It is clear that appropriate VUV radiation, H_2O and OH all coexist in some regions in space. The pump mechanism suggested here is appealing because of its simplicity. We hope, that this model will be of interest to our astrophysics colleagues and will stimulate further modeling.

VI. CONCLUSIONS

This paper contains the results of a detailed investigation of the photodissociation of H_2O in the first absorption band. Measured is the nascent internal state distribution and the alignment of OH both for rotationally cold and warm water. The experimental results are summarized below:

(a) The 2.89 eV of excess energy is partitioned into 88.5% translation, 9.5% vibration, and ~2% into rotation, the latter depending strongly upon parent temperature.

(b) The vibrational distribution is 1:1:0.15 for $v'' = 0$, 1, and 2, respectively.

(c) The OH rotational distributions are nearly Boltzmann from 300 K water, but there are strong deviations from 10K water. The H_2O parent rotation is transferred to the product OH.

(d) The two spin states are nearly statistically populated.

(e) The OH Λ doublets are highly inverted, the degree of inversion increasing rapidly with J_{OH}, and decreasing with initial water temperature.

(f) The measured polarization rates are very large and show a strong J dependence. With increasing water temperature the polarization decreases.

(g) Similar behavior is found in H_2O and D_2O.

Both rotational and vibrational distributions can be explained qualitatively by a discussion for the $^1B_1$ potential surface. The details of the final state interactions are shown to be important by the failure of models in which they are neglected. For cold H_2O we prepare a rather well defined initial state (most particles in the rotational ground state) so that state-to-state fragmentation cross sections are given here.

The high Λ doublet population inversions are responsible for the astronomical OH maser. The inversion is simply explained by symmetry conservation during the fragmentation process. The J dependence of the inversion is explained by the Λ-doublet mixing in OH using a simple one electron model. The degree of the inversion is smeared out by initial H_2O rotations. For the cold H_2O out-of-plane rotations are not important indicating a completely planar dissociation process.

The polarization results can only be interpreted with an appropriate analysis. In the analysis both hyperfine structure *and* Λ-doublet mixing must be taken into account. For the case of cold H_2O the experimental results are in agreement with a completely planar dissociation process. For warm H_2O, out-of-plane rotations cause depolarization. The relatively small depolarization with increasing H_2O temperatures indicates a fast dissociation process.

The data for cold H_2O demonstrates that the dissociation is direct and occurs on a single well-defined potential surface. Because of this simplicity a detailed analysis of the data was possible. Although we have a completely planar dissociation, both Λ-doublet population and polarization show a strong J dependence and only the appropriate analysis reveals this planarity.

The J dependence both for Λ-doublet population and polarization is explained for the first time by Λ-doublet mixing. The J dependence is very different for other Π molecules and depends upon how a fast a molecule goes from Hund's case (a) to Hund's case (b). The simple model presented here should also be applicable to other processes (chemical reactions, surface scattering) with Π molecules.

Note added in proof: The term "Λ-doublet mixing" has to be treated with care in a full quantum treatment. The expansion coefficients c_j and d_j in Eq. (12) are functions of all other coordinates but φ and only $c_j^2 = \langle c_j/c_j \rangle$ and $d_j^2 = \langle d_j/d_j \rangle$ represent the pure numbers given in Eqs. (15) and (18). The proper parity of the states is obtained in Eq. (12) because $|c_j\rangle \rightarrow + |c_j\rangle$ and $|d_j\rangle \rightarrow - |d_j\rangle$ by the parity operation. Also, care has to be taken with the angle φ that is chosen to be 0 if the π lobe is perpendicular to the OH rota-

tion plane. Apart from these minor corrections the treatment given here agrees with the full quantum treatment.

ACKNOWLEDGMENTS

We thank Professor H. Pauly, Director at MPI für Strömungsforschung, for his interest in this work, and GSO and EWR thank him for the opportunity to work as guests there. We thank Professor R. N. Zare for a preprint of Ref. 24, and a computer program for the corresponding polarization analysis and Professor R. N. Dixon for a valuable set of notes on the same subject. We thank Professor V. Staemmler for sending results of *ab initio* calculations on the $^1B_1$ state prior to publication. We thank Professor M. Shapiro, Dr. R. Schinke, and Dr. A. C. Luntz for many helpful discussions and the Deutsche Forschungsgemeinschaft for financial support. EWR thanks the National Science Foundation for partial support.

[1]M. Shapiro and R. Bersohn, Annu. Rev. Phys. Chem. **33**, 409 (1982).
[2](a) J. P. Simons, in *Gas Kinetics and Energy Transfer*, edited by P. G. Ashmore and R. J. Donovan (1977), Vol. 2, p. 58. (b) W. M. Gelbart, Annu. Rev. Phys. Chem. **28**, 323 (1977); (c) J. R. Leone, Adv. Chem. Phys. **50**, 255 (1982).
[3]H. Okabe, *Photochemistry of Small Molecules* (Wiley–Interscience, New York, 1978).
[4]S. Tsurubuchi, Chem. Phys. **10**, 335 (1975).
[5]K. H. Welge and F. Stuhl, J. Chem. Phys. **46**, 2440 (1967).
[6]References may be found in E. Segev and M. Shapiro, J. Chem. Phys. **77**, 5604 (1982).
[7]J. P. Simons and A. J. Smith, Chem. Phys. Lett. **97**, 1 (1983).
[8]P. Andresen, G. S. Ondrey, and B. Titze, Phys. Rev. Lett. **50**, 486 (1983).
[9]See, for example R. S. Berry, S. A. Rice, and J. Ross, *Physical Chemistry*, Part 1 (Wiley, New York, 1980), p. 330.
[10]P. W. Atkins, *Molecular Quantum Mechanics* (Clarendon, Oxford, 1970).
[11]G. Herzberg, *Electronic Spectra and Electronic Structure of Polyatomic Molecules* (Van Nostrand, Princeton, 1967).
[12]See, for example, H.-t. Wang, W. S. Felps, and S. P. McGlynn, J. Chem. Phys. **67**, 2614 (1977).
[13]G. Theodorakopoulos, C. A. Nicolaides, R. J. Buenker, and S. D. Peyerimhoff, Chem. Phys. Lett. **89**, 164 (1982).
[14]D. A. Case, G. M. McClelland, and D. R. Herschbach, Mol. Phys. **35**, 541 (1978).
[15](a) P. J. Dagdigian and R. N. Zare, Science **185**, 793 (1974); (b) J. L. Kinsey, Annu. Rev. Phys. Chem. **28**, 349 (1977).
[16]I. L. Chidsey and D. R. Crosley, J. Quant. Spectrosc. Radiat. Transfer **23**, 187 (1980).
[17]G. H. Dieke and H. M. Crosswhite, J. Quant. Spectrosc. Radiat. Transfer **2**, 97 (1962).
[18]E. A. Moore and W. G. Richards, Phys. Scr. **3**, 223 (1971).
[19]For recent analyses of the OH spectrum, see J. A. Coxon, Can. J. Phys. **58**, 933 (1980); **60**, 41 (1982).
[20]D. H. Levy, L. Wharton, and R. E. Smalley, *Chemical and Biological Applications of Lasers*, edited by C. B. Moore (Academic, New York, 1971), Vol. 2.
[21]D. Dreyfuss and H. Y. Wachman, J. Chem. Phys. **76**, 2031 (1982).
[22]P. Andresen and H. W. Lülf, Rarefied Gas Dynamics (1983).
[23]P. Andresen and E. W. Rothe, Chem. Phys. Lett. **86**, 270 (1982).
[24]C. H. Greene and R. N. Zare, J. Chem. Phys. **78**, 6741 (1983).
[25]P. P. Feofilov, *The Physical Basis of Polarized Emission* (Consultants Bureau, New York, 1961).
[26]E. W. Rothe, F. Ranjbar, D. Sinha, and G. P. Reck, Chem. Phys. Lett. **78**, 16 (1981).
[27]C. H. Greene and R. N. Zare, Annu. Rev. Phys. Chem. **33**, 119 (1982).
[28]P. Andresen and E. W. Rothe, J. Chem. Phys. **78**, 989 (1983).
[29]$D_0(H_2O)$ is from Ref. 3. $D_0(D_2O)$ is calculated from $D_0(H_2O)$ using tabulated zero point energies of H_2O, D_2O, OH, and OD.
[30]G. Herzberg, *Molecular Spectra and Molecular Structure* (Van Nostrand, New York, 1945), Vol. 2.
[31]G. Herzberg, *Molecular Spectra and Molecular Structure* (Van Nostrand, New York, 1950), Vol. 1.
[32]A. D. Wilson and R. D. Levine, Mol. Phys. **27**, 1197 (1974).
[33](a) Y. B. Band and K. F. Freed, Chem. Phys. Lett. **28**, 328 (1974). (b) K. F. Freed and Y. B. Band in *Excited States*, edited by E. C. Lim (Academic, New York, 1977), Vol. 3, p. 109.
[34]K. E. Holdy, L. C. Klotz, and K. R. Wilson, J. Chem. Phys. **52**, 4588 (1970).
[35]R. T. Pack, J. Chem. Phys. **65**, 4765 (1976).
[36]G. N. A. van Veen, K. A. Mohammed, T. Baller, and A. E. de Vries, Chem. Phys. **74**, 261 (1983).
[37]H. Zacharias, M. Geilhaupt, K. Meier, and K. H. Welge, J. Chem. Phys. **74**, 218 (1981).
[38]R. K. Sparks, L. R. Carlson, K. Shobatake, M. L. Kowalczyk, and Y. T. Lee, J. Chem. Phys. **72**, 1401 (1980).
[39]L. C. Lee and D. L. Judge, Can. J. Phys. **51**, 378 (1973).
[40]N.-H. Cheung, J. A. McGarvey, Jr., A. C. Erlandson, and T. A. Cool, J. Chem. Phys. **77**, 5467 (1982).
[41]A. Freedman, S. C. Yang, and R. Bersohn, J. Chem. Phys. **70**, 5313 (1979).
[42]J. A. Beswick and W. M. Gelbart, J. Phys. Chem. **84**, 3148 (1980).
[43](a) W. G. Hawkins and P. L. Houston, J. Chem. Phys. **73**, 297 (1980); (b) **76**, 729 (1982).
[44]A. D. Walsh, J. Chem. Soc. **1953**, 2266.
[45]V. Staemmler, Ruhr Universität Bochum (private communication).
[46]G. S. Ondrey, N. J. A. van Veen, and R. Bersohn, J. Chem. Phys. **78**, 3732 (1983).
[47]R. Vasudev, R. N. Zare, and R. N. Dixon, Chem. Phys. Lett. **96**, 399 (1983).
[48]J. Pfab, J. Häger, and W. Krieger, J. Chem. Phys. **78**, 266 (1983).
[49]W. D. Gwinn, B. E. Turner, W. M. Goss, and G. L. Blackman, Astrophys. J. **179**, 789 (1973).
[50]M. Bertojo, A. C. Cheung, and C. H. Townes, Astrophys. J. **208**, 914 (1976).
[51]J. A. Silver, W. L. Dimpfl, J. H. Brophy, and J. L. Kinsey, J. Chem. Phys. **65**, 1811 (1976).
[52](a) J. F. Córdova, C. T. Rettner, and J. L. Kinsey, J. Chem. Phys. **75**, 2742 (1981). (b) C. R. Rettner, J. F. Córdova, and J. L. Kinsey, *ibid.* **72**, 5280 (1980).
[53]A. C. Luntz, J. Chem. Phys. **73**, 1143 (1980).
[54](a) R. P. Mariella, B. Lantzsch, V. T. Maxson, and A. C. Luntz, J. Chem. Phys. **69**, 5411 (1978); (b) R. P. Mariella and A. C. Luntz, *ibid.* **67**, 5388 (1977); (c) A. C. Luntz, R. Schinke, W. A. Lester, Jr., and Hs. H. Günthard, *ibid.* **70**, 5908 (1979).
[55]P. Andresen and A. C. Luntz, J. Chem. Phys. **72**, 5842 (1980).
[56]A. W. Kleyn, A. C. Luntz, and A. J. Auerbach, Surf. Sci. **117**, 33 (1982).
[57]K. H. Gericke, G. Ortgies, and F. J. Comes, Chem. Phys. Lett. **69**, 156 (1980).
[58]C. Kleinermanns (private communication).
[59]Numerical coefficients for the hyperfine depolarization, obtained with the GZ formulas, were kindly furnished to us by Professor R. N. Dixon, Bristol.
[60]For a recent review on astronomical masers, see M. Elitzur, Rev. Mod. Phys. **54**, 1225 (1982).
[61]M. Shapiro and H. Kaplan, J. Chem. Phys. **71**, 2182 (1979).
[62]However, there is a propensity rule for collisions with a $^2\Pi$ molecules to maintain specific Λ doublets. See M. H. Alexander, J. Chem. Phys. **76**, 5974 (1982).
[63]*Molecules in the Galactic Environment* edited by M. A. Gordon and L. E. Snyder (Wiley–Interscience, NewYork, 1973).
[64]M. Elitzur, University of Kentucky (private communication).
[65]G. P. Glass and B. K. Chaturvedi, J. Chem. Phys. **75**, 2749 (1981).